TECHNICAL REPORT EL-92-32

US Army Corps of Engineers

TERRAIN BACKGROUND SIGNATURE RESEARCH

by

Richard A. Weiss, Randy K. Scoggins, David L. Meeker

Environmental Laboratory

DEPARTMENT OF THE ARMY
Waterways Experiment Station, Corps of Engineers
3909 Halls Ferry Road, Vicksburg, Mississippi 39180-6199

September 1992
Final Report

Prepared for DEPARTMENT OF THE ARMY
US Army Corps of Engineers
Washington, DC 20314-1000

Under DA Project No. 4A162719AT40
Task BO, Work Unit 063

ENVIRONMENTAL LABORATORY

Destroy this report when no longer needed. Do not return
it to the originator.

The findings in this report are not to be construed as an official Department of the Army position unless so designated by other authorized documents.

The contents of this report are not to be used for advertising, publication, or promotional purposes. Citation of trade names does not constitute an official endorsement or approval of the use of such commercial products.

REPORT DOCUMENTATION PAGE

Form Approved
OMB No. 0704-0188

1. AGENCY USE ONLY *(Leave blank)*	2. REPORT DATE	3. REPORT TYPE AND DATES COVERED
	September 1992	Final report

4. TITLE AND SUBTITLE

Terrain Background Signature Research

5. FUNDING NUMBERS

TA BO
WU 063
PR 4A162719AT40

6. AUTHOR(S)

Richard A. Weiss, Randy K. Scoggins, David L. Meeker

7. PERFORMING ORGANIZATION NAME(S) AND ADDRESS(ES)

USAE Waterways Experiment Station, Environmental Laboratory, 3909 Halls Ferry Road, Vicksburg, MS 39180-6199

8. PERFORMING ORGANIZATION REPORT NUMBER

Technical Report
EL-92-32

9. SPONSORING/MONITORING AGENCY NAME(S) AND ADDRESS(ES)

US Army Corps of Engineers, Washington, DC 20314-1000

10. SPONSORING/MONITORING AGENCY REPORT NUMBER

11. SUPPLEMENTARY NOTES

Available from National Technical Information Service, 5285 Port Royal Road, Springfield, VA 22161.

12a. DISTRIBUTION/AVAILABILITY STATEMENT

Approved for public release; distribution is unlimited.

12b. DISTRIBUTION CODE

13. ABSTRACT *(Maximum 200 words)*

This report presents a summary of the multipectral terrain background signature models and battlefield aids that have been developed at the US Army Engineer Waterways Experiment Station as part of a target reconnaissance and surveillance program and as part of a camouflage improvement and evaluation program. A thermal infrared signature model for rough terrain is presented which calculates the surface brightness temperature in terms of local weather conditions, type of terrain texture, thermodynamic parameters of the soil and vegetation, and the root-mean-square height and correlation length of the rough terrain surface.

Radar wave and laser light-scattering models have been developed for rough terrain surfaces. These models predict the scattering cross section, bidirectional reflectance, and depolarizability for realistic terrain surfaces in terms of surface roughness parameters, average dielectric constant, and the

(Continued)

14. SUBJECT TERMS		15. NUMBER OF PAGES
Infrared detectors	Terrain models	95
Target recognition	Terrain radiance	16. PRICE CODE
Temperature	Thermal models	

17. SECURITY CLASSIFICATION OF REPORT	18. SECURITY CLASSIFICATION OF THIS PAGE	19. SECURITY CLASSIFICATION OF ABSTRACT	20. LIMITATION OF ABSTRACT
UNCLASSIFIED	UNCLASSIFIED		

13. (Concluded).

root-mean-square and correlation length of the random dielectric medium that is used to model the volume scattering from terrain backgrounds.

The predicted background signatures are used to develop battlefield aids that include the Regional Thermal Radiance Map, the Regional Radar Scattering Map, and the Regional Laser Reflectance Map, which use color codes to display the thermal and electromagnetic characteristics of potential battlefield areas. Finally, an infrared scene generator is developed which creates a synthetic infrared image of a target located in a three-dimensional terrain background.

PREFACE

The study reported herein was conducted by personnel of the US Army Engineer Waterways Experiment Station (WES). Funding was provided by the Headquarters, US Army Corps of Engineers (HQUSACE), under Department of the Army Project No. 4A162719AT40, Task BO, Work Unit 063, "Electromagnetic Target Surround Characteristics in Natural Terrains." Technical Monitors were LTC R. Payant and MAJ R. Benton, HQUSACE.

This report was prepared by Dr. Richard A. Weiss, Mr. Randy K. Scoggins, and Mr. David L. Meeker of the Environmental Constraints Group (ECG), Environmental Systems Division (ESD), Environmental Laboratory (EL).

The study was conducted under the general supervision of Dr. John Harrison and Dr. John W. Keeley, Director and Assistant Director, EL, respectively, and Dr. Victor C. Barber, Acting Chief, ESD, and under the direct supervision of Mr. Malcolm P. Keown, Chief, ECG.

At the time of publication of this report, Director of WES was Dr. Robert W. Whalin. Commander and Deputy Director was COL Leonard G. Hassell, EN.

This report should be cited as follows:

Weiss, Richard A., Scoggins, Randy K., and Meeker, David L. 1992. "Terrain Background Signature Research," Technical Report EL-92-32, US Army Engineer Waterways Experiment Station, Vicksburg, MS.

CONTENTS

	Page
PREFACE	1
PART I: INTRODUCTION	3
Background	3
Objectives	9
Scope	9
PART II: THERMAL MODELS	10
Two-Dimensional Terrain Surface Temperature Model	10
WES Combined Thermal Model (WESTHERM)	14
PART III: ROUGH TERRAIN SURFACE TEMPERATURE MODEL	21
Model for Solar Illumination on Rough Terrain Surface	22
Sensor View Model	28
PART IV: INFRARED TARGET AND SLOPED TERRAIN MODEL	36
Irradiance on Target and Background	36
Prediction of Target and Background Temperatures	46
Target Facet Radiance	48
Brightness Temperature	50
PART V: THERMAL MODELING OF PETROLEUM, OIL, AND LUBRICANTS BULK STORAGE TANKS	52
Background	52
Mathematical Model	53
PART VI: RADAR SIGNATURES OF TERRAIN BACKGROUNDS	57
PART VII: DEVELOPMENT OF LASER SCATTERING MODELS	61
Background	61
Purpose and Scope	61
Semi-empirical Laser Scattering Model	62
Experimental Calibration of Laser Models	64
PART VIII: BATTLEFIELD AIDS	65
Regional Signature Maps	66
Thermal Infrared Computer Scene Generation	70
Scene Generator Program	78
Camouflage Effectiveness Evaluation System (CEES)	81
PART IX: CONCLUSIONS AND RECOMMENDATIONS	84
Conclusions	84
Recommendations	88
REFERENCES	89

TERRAIN BACKGROUND SIGNATURE RESEARCH

PART I: INTRODUCTION

Background

1. The detection of camouflaged targets that are located in a terrain background generally involves a comparison of the target signature and the terrain background signature. This is the case for active and passive sensors and for all frequency bands in which the sensor operates--microwave (mw), millimeter wave (mmw), infrared (IR), and visible. The magnitude of the target-background signature contrast is used for the prediction of target detection probabilities, for false alarm rates, and for any general estimate of target visibility. Modern technology has provided sophisticated devices that offer increased signature discrimination capabilities that enhance target detection performance. These include radars, forward-looking IR sensors (FLIRS), laser scanners, and target locators.

2. Two main environmental factors determine the target location performance of electromagnetic sensors--terrain and weather. The terrain background environmental factors include soil type, soil moisture, grass, bushes, forest canopies, agricultural development, and urban development. Targets can be camouflaged so as to blend into the terrain background by exhibiting a signature similar to the terrain background signature and having a small target-background signature contrast. Also, targets can be partially or completely hidden from view, as in the case of terrain with sufficiently large mesoroughness due to hills or vegetation such as tall grass, bushes, and trees (Weiss 1981, 1982). Weather conditions often render sophisticated electro-optical sensor systems ineffective. This may be the result of smog, haze, clouds, rain, and snow that obscure a target from a sensor (Kays et al. 1980).

Environmental effects predictions

3. Radar, IR, and laser target detectors are affected by environmental conditions in their own unique ways. Therefore, for a given set of environmental factors, some electromagnetic sensors will operate more efficiently than others, and predicting which system will perform in an optimum way becomes necessary. The basis of these predictions is a complete knowledge of the absorption, emission, scattering, and reflectance of electromagnetic waves from various target and terrain background surfaces, and the transmission and

attenuation of electromagnetic waves through the atmosphere. Only in this way can the electromagnetic target/background signature contrast seen by a distant sensor be predicted in terms of prevailing weather and terrain conditions.

4. A combined experimental and theoretical investigation of the physical phenomena involved in the detection of targets located in complex terrain backgrounds has been undertaken by the US Army Corps of Engineers. This investigation required the development of analytical models that simulate the physical effects of the interaction of electromagnetic waves with the sensor, atmosphere, target, and terrain background. Thus, the effects of weather and terrain on the performance of electromagnetic sensors can be predicted for the time of engagement with the enemy, and the optimum type of electromagnetic sensor can be determined for the expected weather and terrain conditions.

5. The interaction of electromagnetic radiation with the weather structures of the atmosphere and with the various terrain background textures consists of complicated physical processes whose description requires an understanding of the basic physics involved in these processes. Therefore, physics-based analytical models are required to simulate the matter-radiation interaction processes associated with the components of target-detection performance models. These models are necessarily approximations to the real effects that occur in the radiation-environment system, and the user must be aware of the limited validity of the physics models. The user must also be aware of the extreme variability of the terrain background and weather structures, as well as the extreme variability of the associated physical parameters required by the models to make predictions. The main reason for the discrepancies between model predictions of target and terrain background signatures and the actual measured target and terrain background signatures is the lack of accurate knowledge of electromagnetic and thermal parameters of targets, terrain backgrounds, and weather for the time when signature measurements are obtained.

6. Many modern weapon systems operate via a fusion of several types of sensors so that it becomes important to develop models which predict the multispectral appearance of a target in a background and calculate the attenuation of the various modes of electromagnetic energy transfer from the target to the sensor. Acoustic and seismic modes of energy transfer are also possible; however, this report considers only the transfer of energy by electromagnetic waves such as in the case of radar (mmw and mw), thermal FLIRS (0.7100 μm), and laser scanners and visible light cameras (0.4-0.7 μm).

Weather conditions affect the operation of all these devices, and the analytical models that are used for target signature prediction must be multispectral, weather-dependent computer codes.

7. The target detection capability of a sensor is often expressed as a target detection probability that is the product of several component probabilities: for the target/background, for the atmospheric conditions, and for the electromagnetic sensor. The prevailing weather conditions affect both the target/background target detection probability and the atmospheric component of the target detection probability. For instance, the IR target/background contrast is minimized on a rainy day, and the radar returns from wet vegetation often mimic the radar returns from metal targets. An empirical determination of all possible environmental influences on the success of a weapon sensor system is very costly and time consuming; consequently, it is advantageous to use analytical models to predict sensor performance for prevailing weather and terrain conditions.

8. The physical characteristics of terrain backgrounds such as physical temperature, emissivity, absorptivity, heat conductivity, dielectric constant, magnetic permeability, and soil moisture content vary with the time of day and season because of the diurnal and seasonal variation of the insolation and the effects of local weather variations. Therefore, the thermal, radar, and laser signatures of terrain backgrounds will change with weather and season in addition to having a diurnal variation. Target signatures will also experience these changes, and therefore a comprehensive target/background signature model should be able to predict the multispectral contrast between a target and background by simulating the effects of season, weather, and diurnal solar flux variation.

9. The models and algorithms described in this report are designed to be applied to the problem of locating vehicles and high-value targets. Of high value are large critical facilities such as airfields; petroleum, oil, and lubricants (POL) storage tanks; bridges; power plants; and rail yards. Each target will have a characteristic multispectral signature whose contrast with the surrounding terrain background signatures must be predicted at the time of engagement with the enemy.

10. Much work has been done in the area of target-background signature contrast prediction both at the US Army Engineer Waterways Experiment Station (WES) and elsewhere. This report summarizes the WES contribution to multispectral target-background signature simulation with application to thermal

IR, laser, and radar target locators. The physical structure and input parameters of the signature prediction models are described with consideration given to the immense complexity of the problem of forecasting the performance of sophisticated weapon systems.

Framework

11. In addition to a sensor characteristics model and a general systems integration model that combines the basic computer programs, two basic components are needed for an electromagnetic sensor performance prediction model: (a) a target/background model for laser, radar, and laser sensor systems and (b) an electromagnetic and thermodynamic parameter database for targets and terrain backgrounds that will be used to drive the terrain background signature models.

12. Often a target and a terrain background are sufficiently simple so as to be described by a simple signature contrast value for the purpose of target location. For this case, the differences in visible light reflectivity, infrared radiance, and radar cross section can be used to discriminate targets from backgrounds. If, however, the target and terrain background are complex and contain large variations of reflectivity, radiance, and radar cross section, local "hot spots" must be considered on the target and in the terrain background, and the simple concept of signature contrast becomes inadequate to predict target detectability. A statistical analysis of the spatial variation of the background signatures may be of value, but clearly for this case a full scene simulation and an imaging sensor should be used.

13. The signature calculations that would enter a full scene simulation for laser, radar, and thermal IR sensors are performed by describing the unique physical processes that occur when electromagnetic waves in these characteristic wavebands interact with or are transformed by a target and terrain background surface. For laser light interacting with a terrain surface, the relevant processes are surface scattering and reflectance, and a calculation of the bidirectional reflectance is required in terms of frequency, depression angle of the source, and view angle of the sensor. For radar, the relevant processes are scattering and reflection, and the radar differential cross section must be calculated in terms of surface geometry and the electrical parameters of the terrain surface. The calculation of the IR signature of a terrain background requires the evaluation of an energy budget at the terrain surface, which includes all of the relevant modes of energy transfer at the surface. This determines the physical temperature and radiance of the terrain

surface. The modes of energy transfer are determined by the local weather and the thermal properties of the ground.

Environmental parameters
for thermal signature models

14. The primary driving factors that determine the thermal IR signatures of terrain backgrounds are local weather and type of terrain surface, such as soil, vegetation, asphalt runway, etc. The weather affects the amount of solar radiation incident on the terrain surface and therefore can indirectly affect the surface conditions such as water content. Weather directly affects the surface temperature by regulating the incident solar radiation and sky radiation, which is transformed to heat at the terrain surface (Balick et al. 1981). An atmospheric model is needed to determine the amount of attenuation of the background radiance due to absorption and scattering by the atmosphere.

15. The thermal models require their own characteristic terrain background and weather information. The required terrain and geographic data include terrain elevations, soil moisture content, vegetation moisture content, heat conductivity and diffusivity, shortwave absorptivity and longwave emissivity of the terrain surface, latitude of area of interest, and the zenith and azimuth angles of the sun (Balick et al. 1981; Balick, Scoggins, and Link 1981). The weather data include air temperature, cloud cover, cloud type, relative humidity, wind speed, IR sky radiation, and insolation. The weather and terrain background conditions must be known for the precise time of engagement with an enemy target. This is the primary drawback of using analytical models for thermal IR signature prediction because the terrain background parameters are known imprecisely if at all.

16. A prerequisite for the determination of thermal IR images of targets and backgrounds is the prediction of target and background temperatures. Many target and terrain temperature estimation models have appeared in the literature (Kahle 1977; Deardorff 1978; Link 1979; Jacobs 1980; Smith et al. 1980; Balick et al. 1981; Balick, Scoggins, and Link 1981; Botkin et al. 1981; Baird et al. 1982; Hechinger, Raffy, and Becker 1982; Solomon 1982; Hodge 1989). The WES has for several years conducted research on the camouflage of fixed industrial and military installations. This work included a research program for developing a realistic target and surround database for use in the design and evaluation of imaging and nonimaging sensors for surveillance, target acquisition, and terminal homing. A preliminary procedure for

predicting terrain surface temperatures was developed during this research (Link 1979).

17. The prediction of terrain surface temperatures uses an energy budget condition at the ground surface (Kahle 1977, Balick et al. 1981). The effects of insolation, atmospheric IR emission, heat conduction and convection in the air, thermal IR emission from the ground surface, heat conduction in the ground, and latent heat of evaporation and condensation are used to form the energy budget. A one-dimensional (1-D) analysis using this energy budget produced the Terrain Surface Temperature Model (TSTM), which applies to nonvegetative surfaces such as soil, rock, asphalt, and concrete (Balick et al. 1981). Extensions to vegetative canopies have been considered (Deardorff 1978; Smith et al. 1980; Balick, Scoggins, and Link 1981). An initial two-dimensional (2-D) generalization of these heat flow concepts has also been developed for nonvegetated surfaces (Solomon 1982). Several calculations of the temperature of vertical walls have appeared in the literature (Jacobs 1980). An extension of the TSTM to solid and fluid-filled vertical wall targets has also been accomplished (Hodge 1989).

18. An important application of the temperature prediction models is the determination of the thermal IR radiances of targets and backgrounds as a preliminary step for the determination of the apparent IR scenes that would be viewed by a missile seeker (Bornemeier, Bennett, and Horvath 1969; Gillespie and Kahle 1977; Rounds, Zavodny, and Mazzer 1980; Zavodny and Mazzer 1980). A particularly useful thermal-imaging research program is the Air Force Infrared Modeling and Analysis (IRMA) study that developed the computer programs ENVIRON/SCNGEN, which construct a target-in-background IR scene as viewed in the focal plane of the missile seeker optics (Botkin et al. 1981, Baird et al. 1982). ENVIRON calculates target and background temperatures, whereas SCNGEN produces the apparent images of the target and background. The IRMA study has been applied to modeling of military vehicles such as tanks (Botkin et al. 1981, Baird et al. 1982).

19. The environmental information required as input data for models that describe laser light and radar wave scattering from terrain backgrounds consists of weather data, terrain type and land use, terrain roughness, soil and vegetation moisture content, terrain roughness, and the electromagnetic properties of the terrain background such as average dielectric constant, standard deviation of dielectric constant, and the average value and standard deviation of the magnetic permeability. The electromagnetic parameters of

terrain background materials generally depend strongly on the terrain moisture content, which in turn is related to weather and seasonal conditions. The laser light bidirectional reflectance and the radar wave scattering differential cross section can be calculated from these parameters (Ishimaru 1978; Lee and Kong 1985a,b).

20. This report summarizes the terrain and target models and battlefield aids that have been developed at WES to support the US Army high-value target camouflage and target location and surveillance programs. These models have been created to satisfy one of the US Army's key operational capabilities: the detection of enemy targets located in complex terrain backgrounds. Reconnaissance, Surveillance and Target Acquisition and Automatic Target Recognition are rapidly being developed to improve US Army target location capability.

Objectives

21. The objectives of this study were to

a. Summarize WES target and terrain background signature models.

b. Summarize WES battlefield aids.

Scope

22. The scope of this report includes the following:

a. A summary of the thermal signature models developed to predict the physical temperature and radiance of terrain backgrounds.

b. A summary of the rough-surface temperature and radiance prediction model.

c. A description of the target models developed, including fluid-filled targets.

d. The development of radar and laser scattering models for terrain backgrounds.

e. A description of the color-coded regional thermal, laser, and radar terrain signature maps.

f. A summary of the Camouflage Effectiveness Evaluation System.

g. A description of a thermal target and terrain scene generator.

PART II: THERMAL MODELS

Two-Dimensional Terrain Surface Temperature Model

23. The terrain surface temperature model TSTM (Balick et al. 1981), developed by WES, is based upon a finite-difference solution to the thermal diffusion differential equation in one dimension. TSTM is 1-D in the sense that all heat flow is vertical (e.g., down into or up from the soil) with no horizontal effects considered. This assumption is sufficient in many cases where horizontally homogeneous materials are present, such as a farmer's field. Even near edges, 1-D thermal conduction accurately predicts thermal behavior as long as one considers locations at a distance from the edge. However, many situations require modeling the horizontal as well as vertical heat flow, such as on or very near edges or for cases in which a subsurface object is too small to be represented accurately by a 1-D calculation. To overcome these shortcomings of TSTM, a 2-D finite difference thermal model, named TWOD, was developed. This model requires a relatively sparse amount of input data, as in TSTM, but allows simulations of horizontally discontinuous materials.

Model description

24. The terrain temperature model described here represents an extension to the 1-D TSTM model. The model calculates a horizontal as well as vertical temperature profile by determining energy transfer in, out, and through the system. Because the model is 2-D, a basic assumption is that the materials are uniform in the third spatial dimension. TWOD predicts a temperature profile for systems that may be multilayered in both the horizontal and vertical dimensions, as seen in Figure 1 with four materials--A, B, C, and D.

25. Two-dimensional conduction equation. The temperature profiles result from solving the 2-D thermal conduction equation given as

$$\frac{\partial T(x,y,t)}{\partial t} = \alpha(x,y)\left[\frac{\partial^2 T(x,y,t)}{\partial x^2} + \frac{\partial^2 T(x,y,t)}{\partial y^2}\right] \quad (1)$$

where the observable surface is $y = 0$, the lower surface is $y = B$, the left boundary is $x = 0$, and the right boundary is $x = R$. The diffusivity

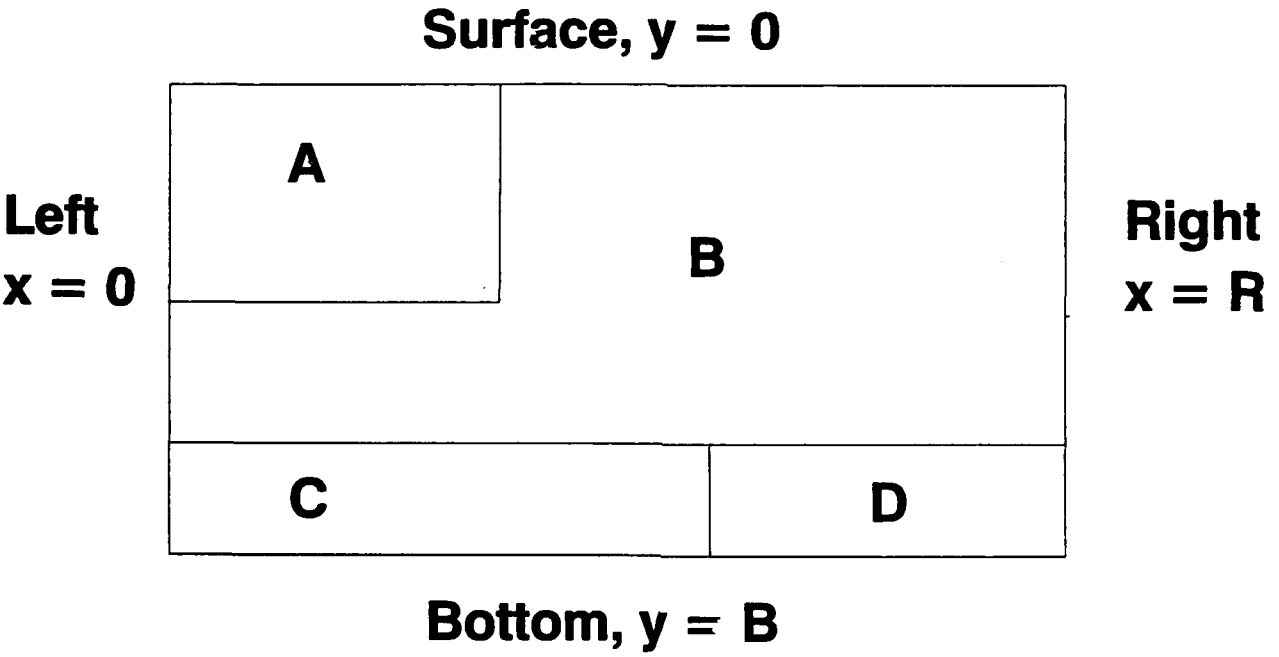

Figure 1. Four-material system

is $\alpha(x,y)$, and b_{it} , l_{jt} , r_{jt} , and B_{it} denote heat fluxes at the appropriate time t at the respective boundary (Solomon 1982).

26. Top surface boundary conditions are calculated in the same manner as in TSTM (Balick et al. 1981) with a single surface boundary condition for all surface materials. This assumes that the most significant heat fluxes at the surfaces are vertical. All other surface boundary conditions are calculated using the parameters of the material present at each boundary grid point specification of one of three conditions at the boundary, as in TSTM. One should note that a combination of different boundary conditions is allowed for the vertical boundaries and the bottom boundary. A grid point is the (x,y) location of a numerical value for the material temperature. Since the numerical solution is discrete and not continuous, the points at which calculations are made define a 2-D grid of points throughout the system.

27. System definition for numerical solution. As stated earlier, the model views the terrain as a plate or finite 2-D slice of a three-dimensional (3-D) terrain. In the case of a multiple material in the vertical and horizontal directions, one must specify the material properties in a manner that may place artificial divisions through a single material. This is necessary for implementation of the 2-D numerical solution. For example, Figure 1 illustrates a system with four materials, but for use with the model, the

system must be specified with nine blocks, as in Figure 2. One of the blocks represents material A, five are specified for material B, two for material C, and one for material D. Thermal parameters are specified for each block by entering the row and column number for each set of parameters. The intent of the relabeling is to view the entire system as a collection of rectangular blocks. Care must be taken to avoid "thin" blocks that may violate the constraints which ensure numerical stability. This states that the product of the diffusivity and the time step divided by the sum of the squares of the horizontal and vertical grid spacings must be less than 1/4 .

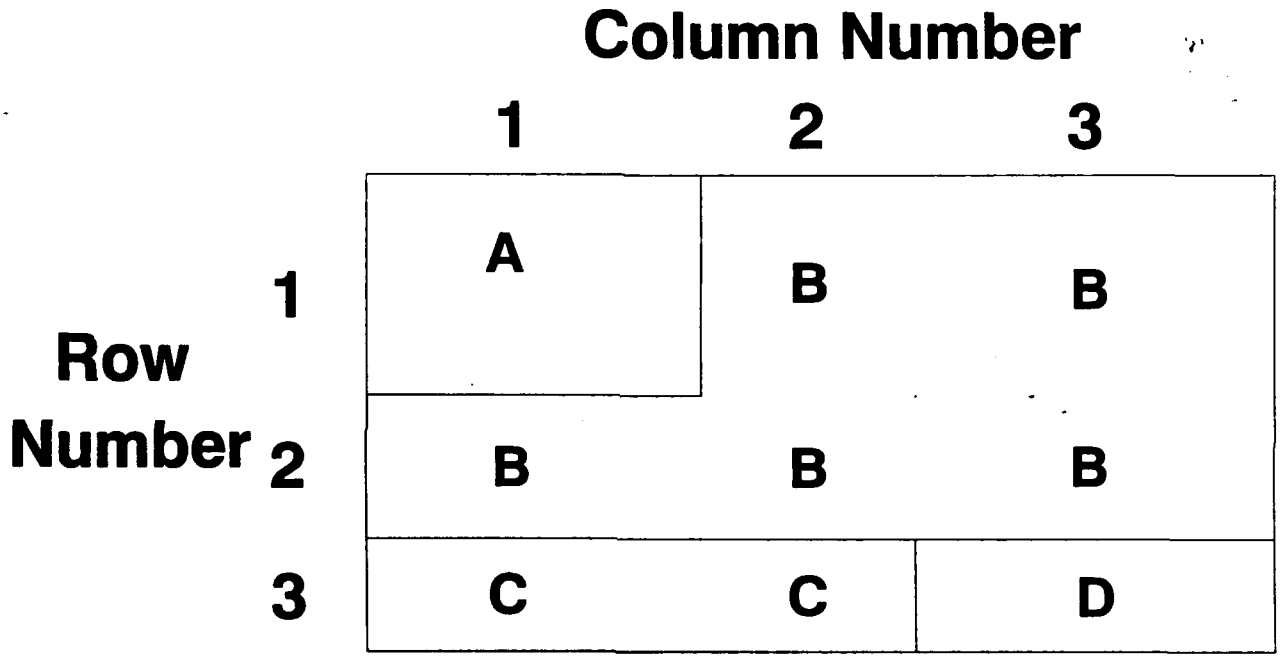

Figure 2. Model specification for four-material system

Numerical solution technique

28. Solution within a block. Within each block, an explicit finite difference scheme is employed to solve the 2-D heat conduction equation (Solomon 1982). Specifically, given the temperature at time t, the new temperature at time $t + \Delta t$ at the grid point (x,y) is given by

$$T(x,y,T+\Delta) = T(x,y,t)$$

$$+ \alpha(x,y)\ (\Delta t)\left[\frac{T(x,y+\Delta y,t) - 2T(x,y,t) + T(x,y-\Delta y,t)}{(\Delta y)^2}\right. \tag{2}$$

$$\left. + \frac{T(x+\Delta x,y,t) - 2T(x,y,t) + T(x-\Delta x,y,t)}{(\Delta x)^2}\right]$$

29. Solution at an interface. Assuming perfect thermal contact between adjacent blocks, the numerical solution equations for heat transfer across vertical and horizontal boundaries of (possibly) dissimilar materials can be derived by the principle of continuity of flux and temperature. This simply states that the heat flux and temperature at a point on the interface must be the same regardless of which side of the interface the flux and temperature are calculated from. Using this principle, equations for temperatures at vertical (Equation 3) and horizontal (Equation 4) interfaces can be derived (Solomon 1982), as given below.

$$\left[\frac{k_A(\Delta x_A)}{2\alpha_A(\Delta t)} + \frac{k_B(\Delta x_B)}{2\alpha_B(\Delta t)}\right] T(x,y,t+\Delta t)$$

$$= \left[\frac{k_A(\Delta x_a)}{2\alpha_A(\Delta t)} + \frac{k_B(\Delta x_B)}{2\alpha_B(\Delta t)}\right] T(x,y,t) + \frac{k_A}{\Delta x_A} T(x-\Delta x,y,t) \tag{3}$$

$$+ \frac{k_B}{\Delta x_B} T(x+\Delta x,y,t) - \left[\frac{k_A}{\Delta x_A} + \frac{k_B}{\Delta x_B}\right] T(x,y,t)$$

$$\left[\frac{k_A(\Delta y_A)}{2\alpha_A(\Delta t)} + \frac{k_B(\Delta y_B)}{2\alpha_B(\Delta t)}\right] T(x,y,t+\Delta T)$$

$$= \left[\frac{k_A(\Delta y_a)}{2\alpha_A(\Delta t)} + \frac{k_B(\Delta y_B)}{2\alpha_B(\Delta t)}\right] T(x,y,t) + \frac{k_A}{\Delta y_A} T(x,y-\Delta y,t) \tag{4}$$

$$+ \frac{k_B}{\Delta y_B} T(x,y+\Delta y,t) - \left[\frac{k_A}{\Delta y_A} + \frac{k_B}{\Delta y_B}\right] T(x,y,t)$$

30. Solution at a corner. Consider the intersection of a horizontal boundary and a vertical boundary, as in Figure 3. Let T'_{AB} denote the new temperature at the (x,y) print at time t + Δt when viewing the configuration as a vertical interface between blocks A and B. Similarly, let T'_{CD} be the new temperature at (x,y) from the point of view of blocks C and D. Define T'_{AC} and T'_{BD} in the same way (Solomon 1982). Then, the new temperature at the corner point (x,y) will be

$$T(x,y,t+\Delta t) = \frac{T'_{AB} + T'_{CD} + T'_{AC} + T'_{BD}}{4} \tag{5}$$

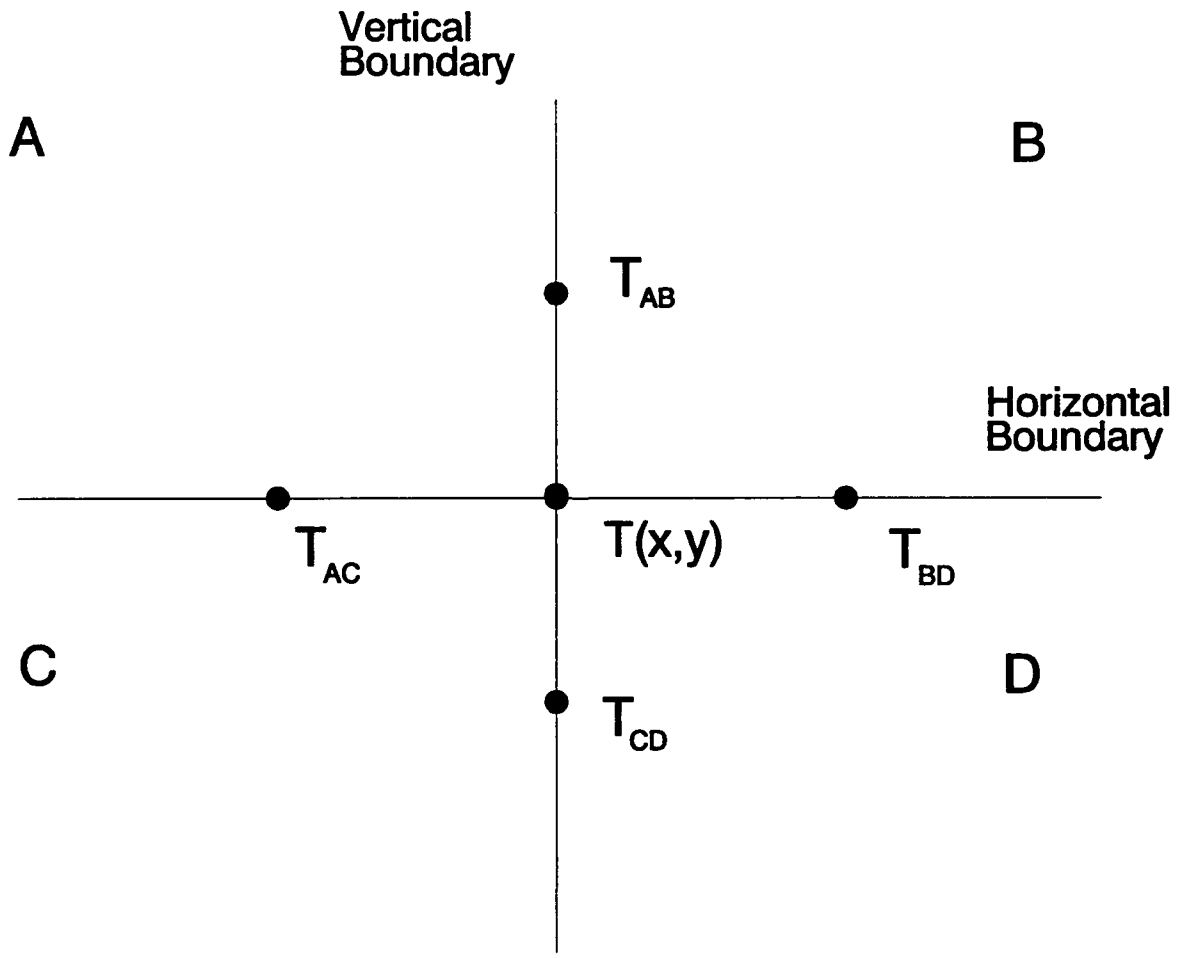

Figure 3. Temperature at vertical-horizontal boundary intersection

WES Combined Thermal Model (WESTHERM)

31. The terrain surface thermal models developed by WES--TSTM for bare surfaces (Balick et al. 1981), VEGIE (Balick, Scoggins, and Link 1981) for short and medium vegetation, and VCTM (Smith et al. 1980) for closed forest canopies--have been used to model surface and vegetation temperatures for generation of surface temperature maps (Weiss and Scoggins 1989), among other applications. TSTM and VEGIE are traditionally described as separate models, even though they constitute different sections of the same program, because they represent two distinct solutions to the surface energy budget of two types of system. Each calculates environmental factors peculiar to the surfaces for which it was designed and passes the correct surface temperature boundary condition to a single solution of the heat conduction equation for propagation of the energy into the ground.

32. Unlike the TSTM-VEGIE program, VCTM is a separate set of programs used to represent a forest canopy as a three-layer system, with additional layers for the ground and sky. One of the shortcomings of VCTM, at least concerning its application to temperature map modeling at WES, is the necessity to provide ground temperature under the canopy as an input. This situation occurs because VCTM does not perform heat conduction calculations for the soil and thus cannot model the ground temperature under the canopy. For initial surface temperature map generation, this deficiency has been circumvented by using VEGIE to model the ground with a high grass cover and then feeding the ground temperature output from VEGIE into VCTM. Such a temporary solution provided a means of estimating forest canopy temperatures but did not address the true physics of the system.

33. To overcome this limitation, VCTM must be combined with the TSTM-VEGIE program in such a way as to allow the calculation of the surface energy budget of the ground under the canopy. This solution requires a coupling of the ground surface temperature to the canopy temperature in addition to the canopy-to-ground coupling that is already present in VCTM. Following is a description of how VCTM was combined with the TSTM-VEGIE program to accomplish this coupling and thus produce a combined surface thermal model (WESTHERM) in which the canopy is coupled with the ground.

Technical approach

34. Background. VCTM models canopy layer temperatures by performing energy budget calculations on each layer (Smith et al. 1980). The energy budget calculations consist of balancing the energy input to a layer against energy lost by the layer. Mechanisms by which energy transfers occur are

Solar radiation (insolation)	- Inputs energy
Atmospheric longwave radiation	- Inputs energy
Canopy layer graybody radiation	- Removes energy
Sensible (convection) transfer	- Inputs and removes energy
Latent (evaporation) transfer	- Inputs and removes energy

These same terms must be calculated at ground level under the canopy to perform the ground-energy budget. Of the five, sensible and latent transfers are by far the most complicated because of the nature of airflow in the canopy. Fortunately, they are probably of lower significance compared with the radiation terms to the undercanopy ground temperature. Therefore, these terms are calculated using the VEGIE equations for a ground surface under medium vegetation, with an appropriate reduction of wind speed under the canopy. The VCTM modification work described here concentrates on the radiation terms of the energy budget that account for the greatest amount of energy transfer.

35. One of VCTM's major strengths is its detailed calculation of radiation incident on the canopy from the sun and atmosphere, and the exchange and/or loss of radiation from the layers because of graybody radiation. These calculations use three sets of parameters calculated by a preprocessor routine that is part of the VCTM package. One of these sets is a matrix $\underline{W}$ of probabilities-of-gap, which is a function of the angle from vertical for the forest canopy used in the solar-loading calculation. The second is a matrix $\underline{S}$ that relates the amount of thermal energy emitted from all layers absorbed by a layer of the canopy. The third set consists of effective shortwave absorptivities for each of the canopy layers. The absorptivities are calculated using a Monte Carlo algorithm that traces the path of light from the source until extinction. Input required for all these calculations includes (for each canopy layer) leaf angle probabilities, leaf area index (LAI), and a 0 to 1 factor describing the degree of leaf clumping. These values can be obtained by measurements or from theoretical distributions. The original preprocessor calculated these values considering the ground as a graybody radiation source only. However, for ground-energy budget calculations, the longwave transfer matrix is modified so that the ground is also a sink for thermal radiation.

36. Longwave radiation calculation. The longwave transfer matrix $\underline{S}$ calculates the amount of energy emitted by each layer (canopy, sky, and ground) absorbed by all three canopy layers, including self-absorption of the canopy layers. The elements of $\underline{S}$ are based on the probability of gaps occurring in each canopy layer and the mean orientation of leaves of a layer (Smith et al. 1980). The gap probabilities are calculated using Equation 6, with N(i) being the LAI of layer i and $g(i,\theta_r)$ the mean leaf area layer i projected in the θ_r direction. This equation assumes that the gap probabilities are independent of azimuth angle ϕ_r .

$$
\begin{aligned}
P(r,\theta_r) &= e^{-N(i)g(i,\theta_r)\sec(\theta)} \\
g(i,\theta_r) &= \int_0^{\pi/2} k(\theta_r,\theta_k)\, f_{ik}\, d\theta_k \\
f_{ik} &= \frac{2}{\pi} \cos(\theta_k) \cos(\theta_r) \;,\; \theta_k \le \frac{\pi}{2} - \theta_r \\
k(\theta_r,\theta_k) &= \frac{4}{\pi^2} \cos(\theta_k) \cos(\theta_r) \left[\phi_k - \frac{\pi}{2} - \tan(\phi_k)\right] \;,\; \theta_k \ge \frac{\pi}{2} - \theta_r \\
\phi_k &= \cos^{-1}\left[-\cot(\theta_k) \cot(\theta_r)\right]
\end{aligned}
\tag{6}
$$

37. Changes in the $\underline{S}$ elements are necessary so that the ground can be a sink or absorbing layer as well as a source layer. Thus, $\underline{S}$ will have five source layers (consisting of the sky, three canopy layers, and the ground) and four sink layers (consisting of three canopy layers and the ground), instead of only the original three canopy layers. The same equation is used to determine the ground-sink $\underline{S}$ probability factors, except that now the orientation of the ground layer replaces the mean leaf orientation and the area projected is unity. Currently, the calculation is made for a horizontal ground, but generalization to arbitrary ground slope is straightforward. Including the ground in the matrix is accomplished by examining the gap probabilities $P(i,\theta_r)$ defined in Equation 7 below. The probability that light will pass through canopy layers and reach the ground is the product of the probabilities-of-gaps for each layer. Since thermal radiation can be emitted and absorbed by the same layer, an additional probability P' is required which is the probability of a gap through one-half the thickness for a given layer. This is given as (Smith et al. 1980)

$$P_1'(r,\theta_r) = \sqrt{P_1(r,\theta_r)} \tag{7}$$

38. To illustrate the overall calculation, consider the probability that thermal radiation from layer 2 will hit the ground from a direction θ_r .

$$P_g(\theta_r) = P(2,\theta_r) \times P(3,\theta_r) - P'(2,\theta_r) \times P(3,\theta_r) \times P(2,\theta_r) \tag{8}$$

39. The total radiation reaching the ground from layer 2 is then found by integrating the radiance contribution from layer 2 over the hemisphere

$$\begin{aligned} L_{2,g} &= 2\pi \times \int_0^{\pi} P_g(\theta) \times L_2 \times | \hat{a} \cdot \hat{r} | \times d\theta \\ &= 2\pi \times L_2 \times \sum_{\theta=0}^{\pi} P_g(\theta) \times C_{ijk} \end{aligned} \tag{9}$$

where L_2 is the radiation of canopy layer 2 as a function of layer temperature and $\hat{a}$ and $\hat{r}$ are the ground normal and source direction unit vectors, respectively. Note that the azimuthal integral is factored out since the probabilities are not a function of azimuth, resulting in the 2π . Since L_2 is considered a constant for a given layer, it can also be brought out of the integral, with the result being the $\underline{S}$ element. In the VCTM preprocessor, the integral is replaced by a sum over discrete sectors approximating the hemisphere, and the parameter C_{ijk} accounts for the area projection of hemispheric sector ij onto layer k. The total energy reaching the ground is then the sum of contributions from this and the other two layers calculated in the same manner. This approach does not account for energy emitted from the ground that is reflected back to the ground, but since leaves have a thermal absorptivity close to one, multiple reflections should not introduce a large error.

40. Solar loading calculation. In addition to the longwave transfer calculation, the ground energy budget requires solar loading, or insolation. Fortunately, the mechanism already exists in VCTM for this calculation. The view angle matrix $\underline{W}$ was originally used to determine the amount of radiation

emitted from the ground and canopy layers that exited the canopy at the top at an angle θ with vertical. This concept can be reversed to calculate the amount of solar radiation that reaches the ground. The calculation requires only those elements of $\underline{W}$ that are used for the ground contribution to the total canopy-emitted radiation. Thus, solar contribution to the ground is broken into two parts: a direct component and a diffuse component. Where available, these components may be entered as input. If only total solar radiation is available, a number representing the fraction of diffuse to direct must be estimated (the default is 0.25).

41. Given direct and diffuse values, total insolation on the ground under the canopy is given by

$$I_{dir} = S_{dir} \times W(4,\theta_{sun}) \tag{10}$$

where I_{dir} and S_{dir} are the insolation and direct solar components, respectively, and $W(4,\theta_{sun})$ is the $\underline{W}$ matrix element for the ground-view factor at the solar elevation angle θ_{sun} .

42. The diffuse contribution requires a summation over the hemisphere and is given by

$$I_{dif} = 2 \times \left[\sum_{\theta=0}^{\frac{\pi}{2}} S_{dif} \times W(4,\theta) \right] \tag{11}$$

where I_{dif} and S_{dif} are the diffuse terms and $W(4,\theta)$ is the term of $\underline{W}$ for discrete values of θ . Note that the summation is over 0 to $\pi/2$ and is multiplied by 2 since the diffuse radiation is considered symmetric about the vertical axis. The total insolation I is then the sum I_{dir} and I_{dif} .

43. Energy budget for the ground. Having calculated the longwave radiation on the ground from the sky and canopy, L , and the total insolation, I, the ground energy budget can be calculated by the approach of TSTM for bare surfaces (Balick et al. 1980). This surface boundary condition is then propagated through the subsurface of the ground by invoking the heat conduction equations of TSTM. By repeated invocation of the modified VCTM module of WESTHERM to calculate undercanopy ground-energy budget and canopy layer

temperatures, the total system can be modeled in the same manner as the VEGIE module of TSTM simulates the effect of short to medium vegetation on surface temperatures.

PART III: ROUGH TERRAIN SURFACE TEMPERATURE MODEL

44. This section describes development of a simple 2-D model for estimating the effects of a rough terrain surface on the values of the background radiance that would be measured by a sensor oriented at a specified depression angle. This is done first, for the case of solar loading, by developing a two-temperature model (for sunlit and shaded areas) that predicts the effective brightness temperature of a rough terrain area. In addition to atmospheric attenuation, the observed background radiance depends on the degree of terrain roughness, texture type, sensor depression angle, solar altitude angle (for insolation), and laser source depression angle for the case of an active laser system. Secondly, a similar model will be developed to describe the ground backscatter from an active laser remote sensing system. Both of these model developments are based on a 2-D calculation in which the source, sensor, and terrain element are in the same plane and only the depression angles of the source and sensor are used. Future development will include an azimuthal angle dependence in order to produce complete 3-D models.

45. The energy flux measured at the sensor originates only from the terrain areas accessible to the sensor's field of view. Some portion of a terrain area may be hidden from view because of the geometry (amplitude and wavelength) of the rough terrain surface; these areas will not contribute to the energy flux measured at the sensor. The procedure for calculating the backscattered radiance of rough terrain, for both solar and laser loadings, involves determining the percent of the viewed terrain surface area that is sunlit or laser illuminated as the case may be. For the case of insolation, the sunlit and shadowed portions of a viewed area contribute different energy fluxes because they have different surface temperatures. For the case of an active laser system, the shadowed portions of the viewed area make no contribution to the energy flux measured at a distant sensor. The bidirectional reflectivity is interpreted to be proportional to the fraction of the viewed area illuminated by laser light. In the following sections, a formalism is developed for determining the fraction of a viewed terrain area that is illuminated or shadowed.

46. The model calculations are performed for sinusoidal terrain surfaces but can be extended to surfaces of arbitrary form by Fourier synthesis. The macroterrain elevations of real surfaces can be obtained from Defense

Mapping Agency databases, the mesoterrain roughness by laser profiling, and the microterrain roughness from soil and vegetation samples.

Model for Solar Illumination on Rough Terrain Surface

47. The apparent terrain background temperature that a sensor measures is generally called the brightness temperature. This temperature differs from the physical temperature of the ground for three reasons: atmospheric attenuation, reflected electromagnetic energy, and rough surface effects. The reduction in surface brightness temperature due to the atmospheric attenuation is modeled by Electro-Optical Systems Atmospheric Effects Library. The effect of reflected energy on the brightness temperature of terrain surfaces has been treated in earlier literature. Weiss and Scoggins (1986) presented a model for predicting the effects of surface roughness on the brightness temperature.

48. The brightness temperature of a rough terrain surface depends on the following factors: solar altitude angle, sensor depression angle, average terrain roughness amplitude, and average terrain roughness wavelength (Bass and Fuks 1979, Carroll 1982, Mahrer 1982, and Weiss and Scoggins 1986). These factors will determine the fraction of the total terrain surface area that is sunlit, the fraction of the total terrain surface area that is viewed by the sensor, and the fraction of the viewed area that is sunlit or shaded. The fraction of the viewed area that is sunlit and shaded, combined with the physical temperatures of the sunlit and shaded areas, is used to calculate the brightness temperature of rough terrain.

49. Initially the terrain surface is assumed to have a sinusoidal variation of elevation. The generalization to surfaces of arbitrary shape can be accomplished by Fourier synthesis. A first step toward calculating the brightness temperature of rough terrain is to determine the fraction of a sinusoidal surface that is sunlit. This is done by referring to Figure 4, which shows the intersection of a sun ray, having a solar altitude angle θ_s, with a terrain elevation sinusoid. The intersection points x_{2s} and x_{3s} shown in Figure 4 can be used to calculate the sunlit and shaded fractions of the terrain surface as follows:

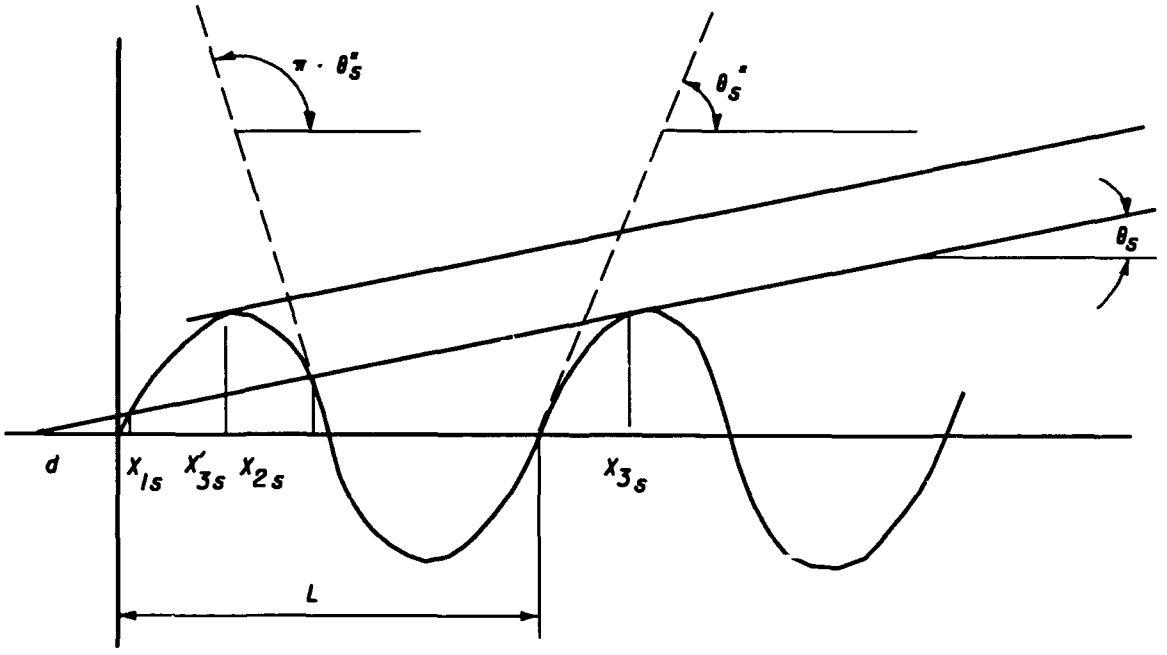

Figure 4. Calculation of illumination function

$$F_s = 1 \qquad \theta_s^* < \theta_s < \frac{\pi}{2} \tag{12}$$

$$F_s = \frac{L + x_{2s} - x_{3s}}{L} \qquad 0 < \theta_s < \theta_s^* \tag{13}$$

$$F_{sh} = 1 - F_s \tag{14}$$

where

F_s - fraction of terrain wavelength that is sunlit

θ_s^* - limiting solar altitude angle beyond which entire terrain surface is sunlit

θ_s - solar altitude

L - wavelength of terrain sinusoid

F_{sh} - fraction of terrain wavelength that is shaded

Therefore, to determine the fraction of sunlit area in terms of the solar altitude angle, the terrain roughness amplitude, and the terrain roughness

wavelength, the intersection points x_{2s} and x_{3s} have to be expressed in terms of these parameters.

50. The calculation of the intersection points x_{2s} and x_{3s} proceeds as follows. The terrain surface sinusoid is written as

$$y = A \sin (kx) \tag{15}$$

where

A = amplitude of terrain roughness sinusoid

k = 2_π/L = wave number of terrain roughness sinusoid

51. The slope of the terrain roughness sinusoid at any point is given by

$$\frac{dy}{dx} = kA \cos (kx) \tag{16}$$

Figure 4 shows that if x'_{3s} is defined as the point of intersection of the tangent sun ray (of slope tan θ_s) with the sinusoid, then

$$\tan \theta_s = kA \cos (kx'_{3s}) \tag{17}$$

$$x_{3s} = L + x'_{3s} \tag{18}$$

so that

$$\begin{aligned} x_{3s} &= L + \frac{1}{k} \cos^{-1} \left(\frac{1}{kA} \tan \theta_s \right) \\ &= L + \frac{1}{k} \tan^{-1} \left(\frac{\sqrt{k^2A^2 - \tan^2\theta_s}}{\tan \theta_s} \right) \end{aligned} \tag{19}$$

52. Equation 19 determines the point x_{3s}. Also from Equation 19 one concludes that the limiting solar angle θ_s^* beyond which the entire surface is sunlit is given by

$$\tan \theta_s^* = kA \tag{20}$$

53. To calculate the point x_{2s}, one writes the equation of the straight line representing the sun ray as follows:

$$y = mx + b \tag{21}$$

where m is the slope and b is the y intercept at $x = 0$ (see Figure 4). The problem is to evaluate m and b in terms of x_{3s}. This is done by first noting that

$$m = \tan \theta_s = \frac{A \sin (kx_{3s})}{d + x_{3s}} \tag{22}$$

where d is the positive value of x intercept at $y = 0$. The value of d can be obtained from Equation 22 to be

$$d = \cot \theta_s A \sin (kx_{3s}) - x_{3s} \tag{23}$$

54. Then, from Figure 4, it follows that

$$b = d \tan \theta_s \tag{24}$$

and therefore,

$$b = A \sin (kx_{3s}) - x_{3s} \tan \theta_s \tag{25}$$

55. The equation of the tangent sun ray is then given by Equations 21, 22, and 25 as

$$y = (x - x_{3s}) \tan \theta_s + A \sin (kx_{3s}) \tag{26}$$

The value y at the point x_{2s} is then given by

$$A \sin (kx_{2s}) = (x_{2s} - x_{3s}) \tan \theta_s + A \sin (kx_{3s}) \tag{27}$$

56. Equation 27 relates x_{2s} and x_{3s} ; therefore, the simultaneous solution of Equations 19 and 27 gives the values of x_{2s} and x_{3s} in the following functional forms:

$$x_{2s} = x_{2s}(L, A, \theta_s) \tag{28}$$

$$x_{3s} = x_{3s}(L, A, \theta_s) \tag{29}$$

57. The simultaneous solution of Equations 19 and 27 is easily obtained numerically using a computer. Then, Equations 13 and 14 determine the sunlit fraction F_s and shaded fraction F_{sh} in terms of L , A , and θ_s .

$$F_s = F_s(L, A, \theta_s) \tag{30}$$

$$F_{sh} = F_{sh}(L, A, \theta_s) \tag{31}$$

Figures 5 and 6 show the dependence of F_s on θ_s and L , respectively.

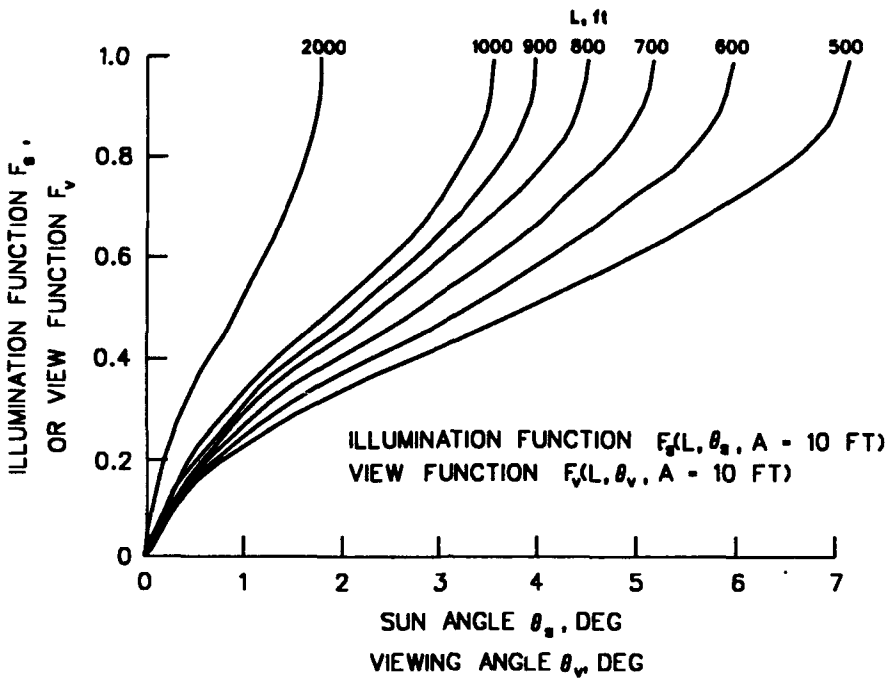

Figure 5. Angular dependence of illumination function

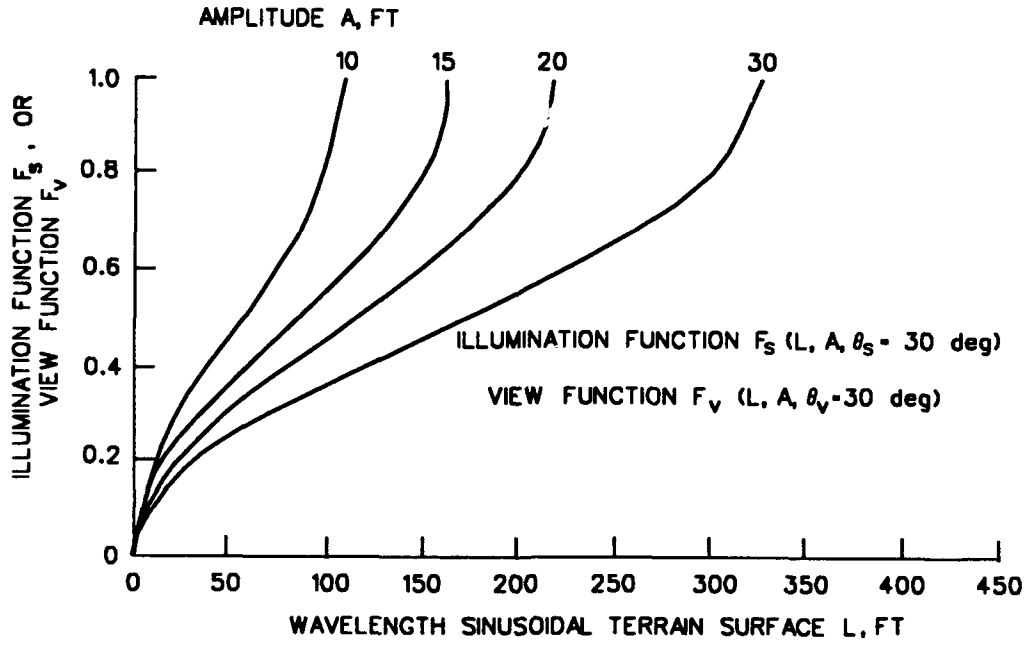

Figure 6. Dependence of illumination function on terrain wavelength

Sensor View Model

58. The construction of a sensor view model requires the development of two capabilities: (a) the prediction of the fraction of the rough terrain area that is viewed by a sensor for a specified depression angle (view altitude angle) and (b) the prediction of the fraction of the viewed area that is sunlit (or illuminated, in the case of laser light). The fraction of the viewed area that is lighted and shaded determines the brightness temperature for solar loading on rough terrain and the bidirectional reflectance for the case of laser illumination of rough terrain.

Fraction of terrain area viewed

59. An analysis similar to that done to calculate the percent of terrain area that is illuminated can be used to calculate the fraction of a rough terrain surface viewed by a sensor. Let θ_v be the view depression angle and x_{2v} and x_{3v} represent intersection points of a view line with the terrain surface sinusoid as shown in Figure 7. Then, the viewed and hidden fractions of a terrain area are expressed as

$$F_v = 1 \qquad \theta_v^* < \theta_v < \pi - \theta_v^* \tag{32}$$

$$F_v = \frac{L + x_{2v} - x_{3v}}{L} \qquad 0 < \theta_v < \theta_v^* \tag{33}$$

$$F_{nv} = 1 - F_v \tag{34}$$

where

F_v = fraction of rough terrain surface that is viewed

θ_v^* = limiting view depression angle beyond which entire terrain surface is viewed

θ_v = view depression angle (view altitude angle)

F_{nv} = fraction of rough terrain surface that is not viewed (hidden)

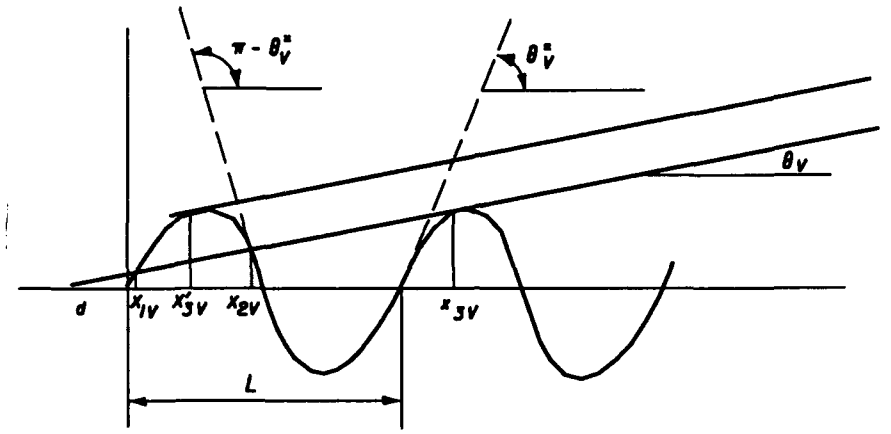

Figure 7. Calculation of viewed area fraction

60. The values of x_{2v} and x_{3v} are obtained in a manner similar to that of x_{2s} and x_{3s} by solving the following simultaneous transcendental equations

$$x_{3v} = L + \frac{1}{k} \tan^{-1}\left(\frac{\sqrt{k^2A^2 - \tan^2\theta_v}}{\tan\theta_v}\right) \tag{35}$$

$$A \sin(kx_{2v}) = (x_{2v} - x_{3v}) \tan\theta_v + A \sin(kx_{3v}) \tag{36}$$

61. These calculations determine x_{2v} and x_{3v} in terms of A , L , and θ_v for $0 < \theta_v < \theta_v^*$, i.e.,

$$x_{2v} = x_{2v}(L, A, \theta_v) \tag{37}$$

$$x_{3v} = x_{3v}(L, A, \theta_v) \tag{38}$$

62. It is clear from Equation 35 that the limiting view angle θ_v^* is given by

$$\tan \theta_v^* = kA \tag{39}$$

such that when $\theta_v^* < \theta_v < \pi - \theta_v^*$, the entire rough terrain sinusoid will be viewed (i.e., there are no hidden areas).

63. For the case when the view angle is opposite to the sun or to the laser source (i.e., when $\pi - \theta_v^* < \theta_v < \pi$), the intersection points of the view line with the terrain surface sinusoid are designated by x_{4v} and x_{5v}. The values of x_{4v} and x_{5v} are given by

$$x_{4v} = \frac{3}{2} L - x_{3v} \tag{40}$$

$$x_{5v} = \frac{3}{2} L - x_{2v} \tag{41}$$

64. The points x_{4v} and x_{5v} are related in this way only for conjugate view lines, i.e., θ_v and $\pi - \theta_v$. For the conjugate view lines, the view fraction is given by

$$F_v = \frac{L + x_{4v} - x_{5v}}{L} \qquad \pi - \theta_v^* < \theta_v < \pi \tag{42}$$

$$= \frac{L + x_{2v} - x_{3v}}{L} \qquad 0 < \theta_v < \pi - \theta_v^* \tag{43}$$

65. Thus, F_v is symmetrical under $\theta_v \rightarrow \pi - \theta_v$. Combining Equations 33-36 and Equation 42 gives the viewed and nonviewed fractions as

$$F_v = F(A, L, \theta_v) \tag{44}$$

$$F_{nv} = F_{nv}(A, L, \theta_v) \tag{45}$$

for $0 < \theta_v < \pi$. The function F_v is the same as F_s that appears in Figures 5 and 6.

Fraction of viewed area illuminated

66. The important physical quantity to calculate for evaluating sensor performance is the fraction of the viewed area that is illuminated, because it is this fraction that determines the effective brightness temperature of rough terrain that a sensor will detect in its field of view, and it is this fraction that determines the bidirectional reflectance for the case of a laser source and detector.

67. Let f_{vs} be the fraction of the viewed area that is illuminated. Since f_{vs} refers both to the source and the viewer, it will in general be a function of both θ_s and θ_v , and can be written in the following functional form:

$$f_{vs} = f_s(A, L, \theta_s, \theta_v) \tag{46}$$

The fraction f_{vs} will be calculated in terms of the intersection points x_{2s} , x_{3s} , x_{2v} , x_{3v} , and also in terms of x_{4v} and x_{5v} for the case $\pi - \theta_v^* < \theta_v < \pi$. This will give the desired result because these intersection points have already been expressed in terms of A , L , θ_s , and θ_v .

68. Figure 8 indicates that the calculation of f_{vs} must be separated into three view angle classes; subsequently, each class must be separated into several subclasses. This is done as follows:

Class I: $0 < \theta_v < \theta_v^*$

$$\textit{Subclass A}: \quad 0 < \theta_v < \theta_s \qquad f_{vs} = 1 \tag{47}$$

$$\textit{Subclass B}: \quad \theta_s < \theta_v < \theta_v^* \qquad f_{vs} = \frac{L + x_{2s} - x_{3s}}{L + x_{2v} - x_{3v}} \tag{48}$$

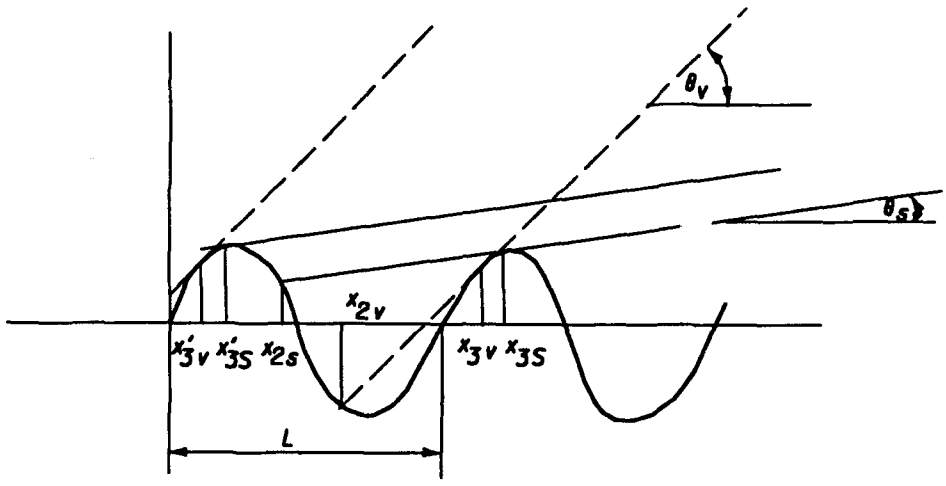

Figure 8. Calculation of fraction of viewed area that is illuminated

Class II: $\theta_v^* < \theta_v < \pi - \theta_v^*$

$$\textit{Subclass A:}\quad \theta_s^* < \theta_s \qquad f_{vs} = 1 \tag{49}$$

$$\textit{Subclass B:}\quad 0 < \theta_s < \theta_s^* \qquad f_{vs} = \frac{L + x_{2s} - x_{3s}}{L} \tag{50}$$

Class III: $\pi - \theta_v^* < \theta_v < \pi$

$$\textit{Subclass A:}\quad x_{2s} < x_{4v} \qquad f_{vs} = \frac{L + x_{2s} - x_{3s}}{L + x_{4v} - x_{5v}} \tag{51}$$

$$\textit{Subclass B:}\quad x_{2s} < x_{4v} \qquad f_{vs} = \frac{L + x_{4v} - x_{3s}}{L + x_{4v} - x_{5v}} \tag{52}$$

$$\textit{Subclass C:}\quad x_{2s} < x_{5v} \qquad f_{vs} = \frac{L + x_{4v} - x_{5v} + x_{2s} - x_{3s}}{L + x_{4v} - x_{5v}} \tag{53}$$

69. The function f_{vs} is not symmetrical under the transformation $\theta_v \rightarrow \pi - \theta_v$. The fraction of the viewed area that is not illuminated is given by

$$f_{vns} = 1 - f_{vs} \tag{54}$$

Figure 9 shows the dependence of f_{vs} on θ_v and θ_s.

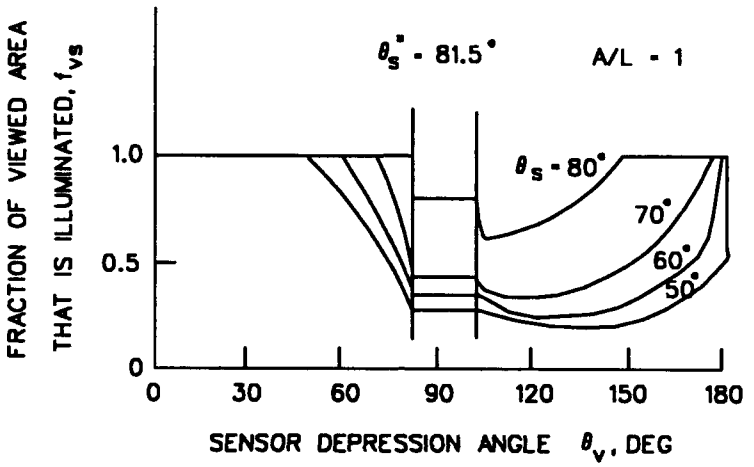

Figure 9. Angular dependence of fraction of viewed area that is illuminated

Effective brightness temperature

70. The effective brightness temperature of rough terrain as observed in the field of view of an infrared sensor can be calculated in terms of the fraction of the viewed area that is sunlit, f_{vs}. Excluding reflected energy, the radiance of the sunlit and shaded portions of a rough terrain area are given respectively by

$$N_s = \frac{\epsilon_s C_1 \Delta\lambda}{\lambda^5 [\exp\ (C_2/(\lambda T_s) - 1]} \tag{55}$$

$$N_{ns} = \frac{\epsilon_{ns} C_1 \Delta\lambda}{\lambda^5 [\exp\ (C_2/(\lambda T_{ns}) - 1]} \tag{56}$$

where

N_s = radiance of sunlit area, W m^{-2} sr^{-1}

ϵ_s = emissivity of sunlit surface

C_1 = 1.192×10^8 W μm^4 m^{-2} sr^{-1}

$\Delta\lambda$ = spectral wavelength interval, μm

λ = weighted average of wavelength, μm

C_2 = 1.434×10^4 μm °K

T_s = temperature of sunlit area, °K

N_{ns} = radiance of shaded area, W m^{-2} sr^{-1}

ϵ_{ns} = emissivity of shaded surface

T_{ns} = temperature of shaded area, °K

71. The average radiance of a rough terrain surface in the field of view of a sensor is given by

$$N = f_{vs} N_s + (1 - f_{vs}) N_{ns} \tag{57}$$

72. Then, the effective brightness temperature is defined by

$$N = \frac{C_1 \Delta\lambda}{\lambda^5 [\exp\ (C_2/\lambda T_{eff}) - 1]} \tag{58}$$

where T_{eff} is the effective brightness temperature. In this way the roughness model determines the following functional dependence:

$$T_{eff} = T_{eff}(A, L, \theta_s, \theta_v, T_s, T_{ns}, \epsilon_s, \epsilon_{ns}, \lambda, \Delta\lambda) \tag{59}$$

73. The terrain amplitude and wavelength, A and L , respectively, can be estimated from statistical terrain roughness parameters (Weiss 1981, 1982). Figure 10 shows an example of the dependence of T_{eff} on the view angle θ_v .

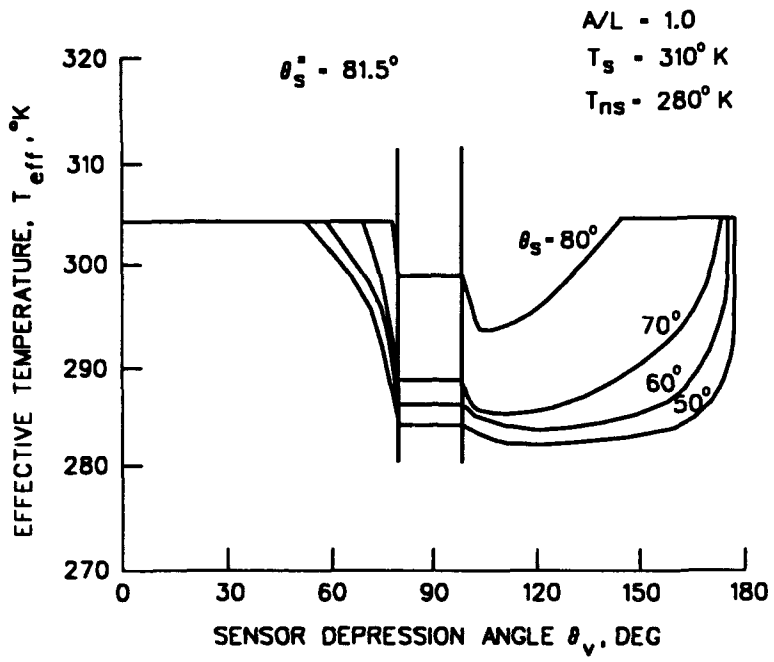

Figure 10. Angular dependence of brightness temperature

PART IV: INFRARED TARGET AND SLOPED TERRAIN MODEL

74. This part of the report describes the procedure for calculating the intrinsic radiance of the target and background surface facets. The procedure involves the calculation of surface temperatures by using an energy budget condition (Budyko 1974). The radiative energy input to this budget for a horizontal surface consists of (a) a short-wave (SW) solar component and (b) a direct longwave (LW) atmospheric component (Balick et al. 1981). For vertical target surfaces, there are three additional components: (a) a SW component reflected from the ground to the target, (b) a LW atmospheric component reflected from the ground to the target, and (c) a LW irradiance on the target resulting from the thermal radiance of the ground. Thus, for a horizontal surface there are two primary radiative power inputs, whereas for a vertical surface there are five. The original TSTM was developed for horizontal surfaces. To use the TSTM for predicting the temperature of a vertical target surface, one must consider the necessary radiative processes associated with a vertical wall (Weiss and Scoggins 1989).

75. Because the IR target and background radiances are generally measured in a specific wavelength interval such as $\Delta\lambda$ = 3-5 or 7-14 μm , the predicted radiances must be calculated for these spectral windows. However, the calculation of the equilibrium target and background surface temperatures requires broadband radiance values. Therefore, both broadband and spectral window radiances are calculated in this report.

Irradiance on Target and Background

Basic photometric definitions

76. The spectral radiance of a target surface is defined as the amount of power radiated per unit area per unit solid angle and per unit wavelength as follows (Holter et al. 1962; Kruse, McGlaughlin, and McQuistan 1962; Jamieson et al. 1963):

$$dP = N_\lambda \cos\theta \, dA \, d\Omega \, d\lambda \tag{60}$$

where

P = emitted power, W

$N\lambda$ = spectral radiance, W m^{-2} μm^{-1} sr^{-1}

θ = angle between direction of observation and the normal to target surface, rad

A = area of target surface, m^2

Ω = solid angle, sr

λ = wavelength, μm

77. The radiance of a surface is defined as

$$N = \int_{\lambda_1}^{\lambda_2} N_\lambda d\lambda, \ W\,m^{-2}\,sr^{-1} \tag{61}$$

and is associated with specified wavelength intervals. The target facet radiances used in TSTM are associated with the 3- to 5-μm and the 7- to 14-μm wavebands.

78. The magnitude of the IR radiance associated with the background and target is due to a number of physical processes associated with the absorption, emission, and reflection of electromagnetic energy. The total IR radiance associated with target and background surfaces consists of a thermal component and a reflected component. The thermal radiance depends on the absolute temperature of the target and background facets.

79. The irradiance H (W m^{-2}) is the electromagnetic power that falls on a unit area of a surface. The radiance, or emissive power, of one surface may impinge on another, thereby becoming an irradiance for the second surface. It is important to distinguish between radiance and irradiance in the calculations shown in this part of the report.

Irradiance on the ground

80. The irradiance on the ground surface consists of the following two terms:

a. Direct SW insolation on ground surface. The SW solar irradiance on the ground is given by (Balick et al. 1981)

$$H_o^g(SW) = S_o W_1 \cos Z_s \tag{62}$$

where

$H_o^g(SW)$ = solar irradiance on ground, W m^{-2}

S_o = solar constant = 1,395.0 W m^{-2}

W_1 = atmospheric transmission factor (Balick et al. 1981)

Z_s = solar zenith angle

b. Direct LW atmospheric irradiance on ground. The broadband atmospheric LW irradiance on the ground is given by the Brunt equation (Balick et al. 1981).

$$H_{atm}^g(LW) = \sigma T_a^4 \left(c + b\sqrt{e_a}\right) \tag{63}$$

where

H_{atm}^g = broadband atmospheric LW irradiance on ground, W m^{-2}

σ = 5.673 × 10^{-8} W m^{-2} °K^{-4}

T_a = ambient air temperature, °K

c,d = empirical coefficients (defined below)

$e_a(T_a,RH)$ = water vapor pressure (Balick et al. 1981)

RH = relative humidity

81. The LW irradiance is diffuse. The $H_{atm}^g(LW)$ function contains empirical coefficients that are chosen to have the values c = 0.73 and b = 0.06 . These values are slightly larger than the values c = 0.61 and b = 0.05 given in Balick et al. (1981). The new values of c and b are chosen because they significantly improve the output of the TSTM when it is applied to various soil types.

82. The Brunt equation is broadband and thus covers all frequencies. The corresponding irradiance on the ground surface in the wavelength interval $\Delta\lambda$ is given by

$$\Delta H_{atm}^g(LW) = \frac{\pi C_1^N \Delta\lambda}{\lambda_{av}^5 \left[\exp\left(\frac{C_2^N}{\lambda_{av} T_a}\right) - 1\right]} \left(c + b\sqrt{e_a}\right) \tag{64}$$

(64)

where

$\Delta H^{\downarrow}_{atm}(LW)$ = spectral window LW irradiance on ground, W m^{-2}

C_1^N = 1.192 × 10^8 W μm^4 m^{-2} sr^{-1}

$\Delta\lambda$ = wavelength interval = 7 and 2 μm, respectively

C_2^N = 1.4338 × 10^4 μm °K

λ_{av} = weighted average wavelength; in the spectral window 7 to 14 μm = 10.76 μm, and for 3 to 5 μm = 4.8 μm

Irradiance on a vertical target facet

83. The TSTM was originally designed to predict the ground surface temperature or the temperature of a horizontal surface. This model has been modified to describe vertical surfaces by including the important radiative interchanges between the vertical target, the atmosphere, and the background.

84. The radiative transfer at the target surfaces has LW and SW components and includes five major irradiance components, as described in the following paragraphs.

85. Direct SW insolation on target. The direct SW solar irradiance on a target surface is given by

$$H_o^{tar}(SW) = S_o W_1 \cos \phi_t \tag{65}$$

where

$H_o^{tar}(SW)$ = solar irradiance on target surface, W m^{-2}

ϕ_t = angle between surface normal and direction of the sun

86. A simple analysis shows that (Balick et al. 1981)

$$\cos \phi_t = \sin Z_s \sin (SL) \cos (S_{AZ} - SL_{AZ}) + \cos Z_s \cos (SL) \tag{66}$$

where

SL = slope angle of target surface

S_{AZ} = solar azimuth angle

SL_{AZ} = azimuth angle of normal to target surface

87. The result in Equation 66 follows from the fact that the unit vector normal to the surface of the target is

$$\hat{n}_t = \hat{I} \sin (SL) \cos (SL_{AZ}) + \hat{J} \sin (SL) \sin (SL_{AZ}) + \hat{K} \cos (SL) \tag{67}$$

and the unit vector in the direction of the sun is given by

$$\hat{n}_s = \hat{I} \sin Z_s \cos S_{AZ} + \hat{J} \sin Z_s \sin S_{AZ} + \hat{K} \cos Z_s \tag{68}$$

88. By the definition of the scalar product, it follows that

$$\begin{aligned} \cos \phi_t &= \hat{n}_t \cdot \hat{n}_s \\ &= \sin (SL) \sin Z_s [\cos (SL_{AZ}) \cos S_{AZ} \\ &\quad + \sin (SL_{AZ}) \sin S_{AZ}] + \cos (SL) \cos Z_s \\ &= \sin Z_s \sin (SL) \cos (S_{AZ} - SL_{AZ}) + \cos Z_s \cos (SL) \end{aligned} \tag{69}$$

This is the same result as in Equation 66.

89. SW solar radiation reflected from background to target. The SW irradiance on the target surface due to specularly reflected insolation from the ground is given by

$$H^{tar}_{ref,g}(SW) = r_g(SW) S_o W_1 \cos^2 Z_s \cos \phi^R_t \tag{70}$$

where

$r_g(SW)$ = SW reflected coefficient of ground = 1 - $\epsilon_g(SW)$

$\epsilon_g(SW)$ = SW absorptivity of ground

ϕ^R_t = angle between surface normal and the reflected sun ray

90. For diffuse reflection of solar insolation from the ground, the SW irradiance on the target surface is given by

$$H_{ref,g}^{tar}(SW) = \frac{1}{\pi} r_g(SW) S_o W_1 G \cos Z_s \tag{71}$$

where G is the radiation configuration factor that will be defined later. If the ground is taken to be infinite half-plane, then $G = \pi/2$.

91. Simple geometry shows that

$$\cos \phi_t^R = \sin Z_s \sin (SL) \cos (S_{AZ} - SL_{AZ}) - \cos Z_s \cos (SL) \tag{72}$$

The result in Equation 72 is obtained by calculating the scalar product between the unit vector normal to the target surface and the unit vector in the (negative) direction of the reflected sun ray. The unit vector in the (negative) direction of the reflected sun ray is given by

$$\hat{n}_s^R = \hat{I} \sin Z_s \cos S_{AZ} + \hat{J} \sin Z_s \sin S_{AZ} - \hat{K} \cos Z_s \tag{73}$$

92. By definition it follows that

$$\begin{aligned} \cos \phi_t^R &= \hat{n}_t \cdot \hat{n}_s \\ &= \sin (SL) \sin Z_s [\cos (SL_{AZ}) \cos S_{AZ} \\ &\quad + \sin (SL_{AZ}) \sin S_{AZ}] - \cos Z_s \cos (SL) \\ &= \sin (SL) \sin Z_s \cos (S_{AZ} - SL_{AZ}) - \cos Z_s \cos (SL) \end{aligned} \tag{74}$$

This is just the result given in Equation 72.

93. Direct LW atmospheric irradiance on target surface. The broadband atmospheric IR irradiance on a horizontal target surface is assumed to be given by the Brunt equation as in the case of the LW irradiance on the ground (Equation 63).

$$H_{atm}^{tar}(LW) = H_{atm}^{g}(LW) \tag{75}$$

where $\Delta H_{atm}^{tar}(LW)$ is the direct broadband LW irradiance on target surface, in W m^{-2}.

94. For a vertical target surface, the broadband atmospheric IR irradiance is given by

$$H_{atm}^{tar}(LW) = \frac{1}{2} H_{atm}^{g}(LW) \tag{76}$$

The corresponding atmospheric irradiance on the horizontal target surface in a spectral range is assumed to be the same as spectral atmospheric irradiance on the ground, as given by Equation 64, so that

$$\Delta H_{atm}^{tar}(LW) = \Delta H_{atm}^{g}(LW) \tag{77}$$

where $\Delta H_{atm}^{tar}(LW)$ is the spectral window LW atmospheric irradiance on the target, in W m^{-2}.

95. For a vertical target surface, the atmospheric spectral irradiance is given by

$$\Delta H_{atm}^{tar}(LW) = \frac{1}{2} \Delta H_{atm}^{g}(LW) \tag{78}$$

96. LW atmospheric radiation reflected from ground to target. Because the atmospheric LW radiation is diffuse in nature, the radiation reflected from the ground will also be diffuse, and the LW broadband irradiance on a raised target surface is given by (General Electric Company 1975)

$$H_{ref,g}^{tar}(LW) = \frac{1}{A_t} \iint \frac{N_{ref}^{g}(LW) \cos \theta_t \cos \theta_g}{r^2} dA_g \, dA_t \tag{79}$$

where the diffuse reflected LW ground radiance is given by

$$N^{g}_{ref}(LW) = \frac{r_g(LW)}{\pi} H^{g}_{atm}(LW) \tag{80}$$

and where $H^{s}_{atm}(LW)$ is given by Equation 63 and

A_t = target area

θ_t = angle between normal to target and reflected ray

θ_g = angle between normal to ground and incident ray

r = variable distance between points on ground and on target surface

A_g = area of ground

$r_g(LW)$ = LW reflectively of ground = 1 - $\epsilon_g(LW)$

$\epsilon_g(LW)$ = LW absorptivity of ground = LW emissivity of ground

97. For the case when the thermal ground radiance $N^{s}_{ther}(LW)$ is independent of the position in the ground plane, the integral in Equation 79 can be evaluated analytically with the result that, for a half-plane,

$$H^{tar}_{ref,g}(LW) = GN^{g}_{ref}(LW) \tag{81}$$

where (General Electric Company 1975)

$$G = \tan^{-1}(b/c) - \frac{c}{\sqrt{a^2 + c^2}} \tan^{-1}\left(\frac{b}{a^2 + c^2}\right) \tag{82}$$

and

a,b = length and width, respectively, of quarter-plane

c = vertical height of observation point on vertical target wall

98. For the case of a homogeneous semi-infinite half-plane background, $G = \pi/2$, Equation 81 becomes

$$H^{tar}_{ref,g}(LW) = \frac{\pi}{2} N^{g}_{ref}(LW) \tag{83}$$

99. The corresponding reflected LW atmospheric radiation in the 7- to 14-μm waveband is obtained from Equations 80 and 81 to be

$$\Delta H^{tar}_{ref,g}(LW) = G\Delta N^{g}_{ref}(LW) \tag{84}$$

where

$$\Delta N^{g}_{ref}(LW) = \frac{r_g(LW)}{\pi}\ \Delta H^{g}_{atm}(LW) \tag{85}$$

and $\Delta H^{g}_{atm}(LW)$ is given by Equation 64.

100. LW irradiance on target due to thermal radiance of the ground. The diffuse LW irradiance on a raised target due to the thermal radiance of the ground is given by (General Electric Company 1975)

$$H^{tar}_{ther,g}(LW) = \frac{1}{A_t}\iint \frac{N^{g}_{ther}(LW)\ \cos\theta_t \cos\theta_g}{r^2}\ dA_g\ dA_t \tag{86}$$

where the broadband thermal ground radiance is obtained from Planck's law as

$$\begin{aligned} N^{g}_{ther}(LW) &= \epsilon_g(LW)\, C_1^N \int_0^{\infty} \frac{d\lambda}{\lambda^5\left[\exp\left(\frac{C_2^N}{\lambda T_g}\right) - 1\right]} \\ &= \epsilon_g(LW)\ \frac{\sigma\ T_g^4}{\pi} \end{aligned} \tag{87}$$

and

$C_1^N = 1.192 \times 10^8$ W μm^4 m^{-2} sr^{-1}

$C_2^N = 1.4338 \times 10^4$ μm °K

$\sigma = 5.673 \times 10^{-8}$ W m^{-2} $°K^{-4}$

T_g = ground temperature, °K

101. For the case of a homogeneous half-plane background, the integral in Equation 86 simplifies to

$$H^{tar}_{ther,g}(LW) = G\, N^{g}_{ther}(LW) \tag{88}$$

where the geometry factor G is given by Equation 82.

102. The corresponding spectral radiance of the ground is given by Equation 86 with $N^{g}_{ther}(LW)$ replaced by

$$\Delta N^{g}_{ther}(LW) = \epsilon_g(LW)\, C_1^N \int_{\lambda_1}^{\lambda_2} \frac{d\lambda}{\lambda^5 \left[\exp\left(\frac{C_2^N}{\lambda T_g}\right) - 1\right]}$$

$$= \frac{\epsilon_g(LW)\; C_1^N\, \Delta\lambda}{\lambda_{av}^5 \left[\exp\left(\frac{C_2^N}{\lambda_{av} T_g}\right) - 1\right]} \tag{89}$$

103. For the case of a homogeneous half-plane background, the spectral irradiance on the target due to the thermal ground radiance is obtained from Equation 88 to be

$$\Delta H^{tar}_{ther,g}(LW) = G\Delta N^{g}_{ther}\ (LW) \tag{90}$$

104. Less important radiative transfer effects are

a. Shortwave solar radiation reflected from target surface to the background and reradiated as IR thermal emittance, which irradiates the target.

b. Atmospheric IR radiation reflected from target surface to the background and reradiated as a thermal IR emittance, which in turn irradiates the target.

105. The total SW irradiance on the target surface is obtained from Equations 65 and 70 to be

$$H^{tar}(SW) = H^{tar}_{o}(SW) + H^{tar}_{ref,g}(SW) \tag{91}$$

The total LW irradiance on the target surface is obtained from Equations 75, 79, and 86 to be

$$H^{tar}(LW) = H^{tar}_{atm}(LW) + H^{tar}_{ref,g}(LW) + H^{tar}_{ther,g}(LW) \quad (92)$$

106. For horizontal surfaces such as the ground, the target irradiances given in Equations 91 and 92 reduce to those given in Equations 62 and 63, respectively.

107. The absorbed part of the total irradiance on a target surface enters the calculation of the target surface temperature. The absorbed power per unit area is obtained from Equations 91 and 92 as

$$H^{tar}_{abs} = \epsilon_t(SW) H^{tar}(SW) + \epsilon_t(LW) H^{tar}(LW) \quad (93)$$

where

H^{tar}_{abs} = power absorbed per unit area, W m^{-2}

$\epsilon_t(SW)$ = SW absorptivity of target surface = SW emissivity

$\epsilon_t(LW)$ = LW absorptivity of target surface = LW emissivity

108. It is this total absorbed power that enters the calculation of target facet temperature using the computer program TSTM. The procedure for calculating the target surface temperature using Equation 93 is essentially the same as used for calculating the ground temperature.

109. For surfaces that are not horizontal, the orientation of the surface with respect to the direct and reflected radiation components enters the irradiance calculation. This introduces a dependence of the predicted target surface temperature on the slope and azimuth angles of the surface and a dependence on the solar zenith and solar azimuth angles.

Prediction of Target and Background Temperatures

110. The equilibrium surface temperature is determined by satisfying an energy flow budget equation at the surface of a target or background (Budyko 1974, Balick et al. 1981). The power input includes the absorption of a SW insolation component and a LW atmospheric term as given by Equation 93.

Energy flow budget

111. The surface temperature of the target and background is calculated using the power budget of the TSTM computer program (Balick et al. 1981). Several physical processes are included in this model:

a. Radiative absorption at the surface (Equation 93).

b. Thermal emission from the surface.

c. Conduction of heat in the solid background or solid target.

d. Conduction and convection by the atmosphere.

e. Latent heat of evaporation.

The energy flow budget for solid targets and backgrounds has been fully described (Balick et al. 1981).

Convection and conduction in fluids and solids

112. In the energy budget of the original TSTM, heat conduction is the mode of energy transfer into a solid target or background. However, heat convection is the dominant heat transfer process in fluid-filled targets such as petroleum storage tanks. Therefore, in order to use the TSTM computer program for petroleum storage tanks, the actual heat convection process must be converted to an equivalent heat conduction problem.

113. The heat conduction process is described by two parameters: heat conductivity and thermal diffusivity. Thermal diffusivity is defined as follows (Hodge 1989):

$$\alpha = \frac{k}{\rho C_p} \tag{94}$$

where

α = thermal diffusivity, $cm^2\ min^{-1}$

k = thermal conductivity, $cal\ (cm\ min\ °K)^{-1}$

ρ = mass density of solid, g mass cm^{-3}

C_p = specific heat at constant pressure, $cal\ (g\ °K)^{-1}$

114. The heat conduction equation in one dimension is (Hodge 1989)

$$\frac{\partial T}{\partial t} = \alpha \frac{\partial^2 T}{\partial \chi^2} \tag{95}$$

where

T = temperature, °K

t = time

χ = distance, cm

115. Equation 95 is a diffusion equation that describes the transfer of heat by the spreading of molecular agitation in a lattice. This description is adequate for solids but not for fluids like gases and liquids whose molecules are free to move in bulk flows.

116. For fluids, convective heat transfer totally dominates the heat conduction process. Equation 95 and its solutions are not applicable to heat convective processes. In fact, the convective heat transfer equation is

$$\frac{\partial T}{\partial t} + u \frac{\partial T}{\partial \chi} = \alpha \frac{\partial^2 T}{\partial \chi^2} \tag{96}$$

where $u = u(\chi,t)$ = fluid speed . The solution of Equation 96, the continuity equation, and the Navier-Stokes equations yields the temperature and fluid velocity distribution in the fluid. The solution of these three equations is difficult for realistic fluids, and a simpler engineering solution to the convection problem that utilizes Equation 95 with an effective conductivity is applied (Hodge 1989).

Target Facet Radiance

117. The total IR emittance from a target or background surface in a wavelength interval $\Delta\lambda$ is the sum of a reflected IR component and a thermal IR emittance calculated from the predicted target surface temperature.

Thermal IR radiance of target

118. The thermal radiance of a target or background surface in a wavelength interval $\Delta\lambda$ is calculated from Planck's blackbody radiation law as follows

$$\Delta N_{ther}^{tar}(LW) = \epsilon_t(LW)\, C_1^N \int_{\lambda_1}^{\lambda_2} \frac{d\lambda}{\lambda^5 \left[\exp\left(\frac{C_2^N}{\lambda T_t}\right) - 1 \right]}$$

$$= \frac{\epsilon_t(LW)\, C_1^N\, \Delta\lambda}{\lambda_{av}^5 \left[\exp\left(\frac{C_2^N}{\lambda_{av} T_t}\right) - 1 \right]} \qquad (97)$$

where

ΔN_{ther}^{tar} = thermal radiance of target, W m^{-2} sr^{-1}

T_t = target surface temperature, °K

119. The atmospheric IR transmission windows are 3 to 5 μm and 7 to 14 μm. The important parameters for the determination of thermal radiance are the target surface temperature, the emissivity of the surface, and the transmission wavebands.

Reflected IR radiance

120. In addition to the thermal IR radiance of a surface, there is a reflected IR radiance in a wavelength interval $\Delta\lambda$, which for a vertical surface is due in part to the IR atmospheric radiation reflected directly from the target and in part to the IR atmospheric radiation reflected from the background and then reflected again from the target surface. There is also an IR reflected component due to the thermal emittance of the background, which is reflected by the target surface. The total reflected radiance in a wavelength interval $\Delta\lambda$ is calculated from the total irradiance on the target surface in the wavelength interval $\Delta\lambda$, which is obtained from Equations 77, 84, and 90 to be

$$\Delta H^{tar}(LW) = \Delta H_{atm}^{tar}(LW) + \Delta H_{ref,g}^{tar}(LW) + \Delta H_{ther,g}^{tar}(LW) \qquad (98)$$

121. The reflected IR radiance in the wavelength interval $\Delta\lambda$ is calculated, under the assumption that it is diffuse, in the following manner:

$$\Delta N_{ref}^{tar}(LW) = \frac{r_t(LW)}{\pi} \Delta H^{tar}(LW) \quad (99)$$

where $r_t(LW)$ = LW reflectivity = $1 - \epsilon_t(LW)$.

Total target and ground radiance

122. The total target facet IR radiance in the wavelength interval $\Delta\lambda$ is obtained finally as the sum of the thermal radiance and the LW reflected radiance as follows:

$$\Delta N^{tar}(LW) = \Delta N_{ther}^{tar}(LW) + \Delta N_{ref}^{tar}(LW) \quad (100)$$

where $\Delta N_{ther}^{tar}(LW)$ is given by Equation 97. This is the intrinsic target radiance that serves as input for the determination of the apparent radiance seen by the IR detector.

123. The ground radiance can be obtained from Equations 98 through 100 as a special case

$$\Delta H^{g}(LW) = \Delta H_{atm}^{g}(LW) \quad (101)$$

$$\Delta N_{ref}^{g}(LW) = \frac{r_g(LW)}{\pi} \Delta H^{g}(LW) \quad (102)$$

$$\Delta N^{g}(LW) = \Delta N_{ther}^{g}(LW) + \Delta N_{ref}^{g}(LW) \quad (103)$$

where $r_g(LW) = 1 - \epsilon_g(LW)$ and where $\Delta H_{atm}^{g}(LW)$ and $\Delta N_{ther}^{g}(LW)$ are given by Equations 64 and 89, respectively.

Brightness Temperature

124. A blackbody brightness temperature for a target such as a POL tank can be associated with a radiance value as follows:

$$T^B = \frac{C_2^N}{\lambda_{av} \ln\left(1 + \frac{C_1^N \Delta\lambda}{\Delta\bar{N} \lambda_{av}^5}\right)} \qquad (104)$$

where

T^B = brightness temperature, °K

$C_2^N = 1.4338 \times 10^4$ μm °K

$C_1^N = 1.192 \times 10^8$ W μm^4 m^{-2} sr^{-1}

ΔN = average apparent radiance of target, W m^{-2} sr^{-1}

$\Delta\lambda$ = wavelength window, μm

λ_{av} = weighted average wavelength in window $\Delta\lambda$

In this way, a temperature can be associated with each of the average radiances that have been defined for a target.

PART V: THERMAL MODELING OF PETROLEUM, OIL, AND LUBRICANTS BULK STORAGE TANKS

Background

125. Reliable models are available that can predict the thermal surface conditions for grass- and vegetation-covered surfaces (Balick, Scoggins, and Link 1981) as well as for bare soil and concrete (Balick et al. 1981). Complementary thermal surface-condition models for fixed-installation targets such as POL bulk storage tanks are needed but are not generally available. Because POL storage tanks are high-asset targets and because modeling methodology appropriate for these tanks could also be used for other fixed-installation targets, POL tanks were chosen as the target to be thermally modeled.

126. The objective of this effort was the preliminary development and validation of a thermal model to realistically predict the surface temperature histories of POL bulk storage tanks. To possess sufficient fidelity, such a model must account for external factors such as air temperature, solar insolation, wind, and cloud conditions as well as internal convection and storage effects. As with the Terrain Surface Temperature Model (Balick et al. 1981), a premium was placed on simplicity and flexibility. A model with these characteristics must consider and emulate the dominant physical phenomena that influence the surface temperatures.

127. A simple but physically realistic model to predict the temperature time-dependence of the external surfaces on POL bulk storage tanks is summarized in this section (Hodge 1989). Model development is first considered in terms of the physical phenomena that influence the temperatures of each of the surfaces, and from these considerations the physical bases of the overall model are selected. The WES vertical wall target model was used to calculate the radiant energy flux on the target wall (Weiss and Scoggins 1989).

128. A lumped-mass surface-temperature thermal model for POL bulk storage tanks is developed. The model uses 12 ordinary, coupled, first-order differential equations, obtained from energy balances, to describe the time-dependent variation of the surface temperatures of a partially filled POL tank. Convective heat transfer and direct and diffuse irradiation are modeled as energy transfers into and out of the 12 lumped masses. One-dimensional transient conduction is considered in the soil below the tank. The model is

implemented in a computer simulation. Comparisons of the predicted tank surface temperatures with the limited data available show that the correct trends and salient features are predicted. In most instances, predicted temperatures are within a few degrees Celsius of measured. Preliminary model performance indicates that the technique incorporates much of the correct physics and is capable of being developed into a reliable, predictive model (Hodge 1989).

Mathematical Model

129. An examination of important physical phenomena that determine the temperature of various POL bulk storage tank surfaces is a necessary first step in devising an adequate predictive simulation. Figure 11, a cross section of a POL storage tank and its surroundings, schematically illustrates the pertinent energy transfer mechanisms. The tank is partially filled with some liquid, typically a petroleum-based product. An air space exists between the liquid and the tank top. The tank surface temperatures are determined by the response of the tank, liquid, and air masses to the energy transferred to or

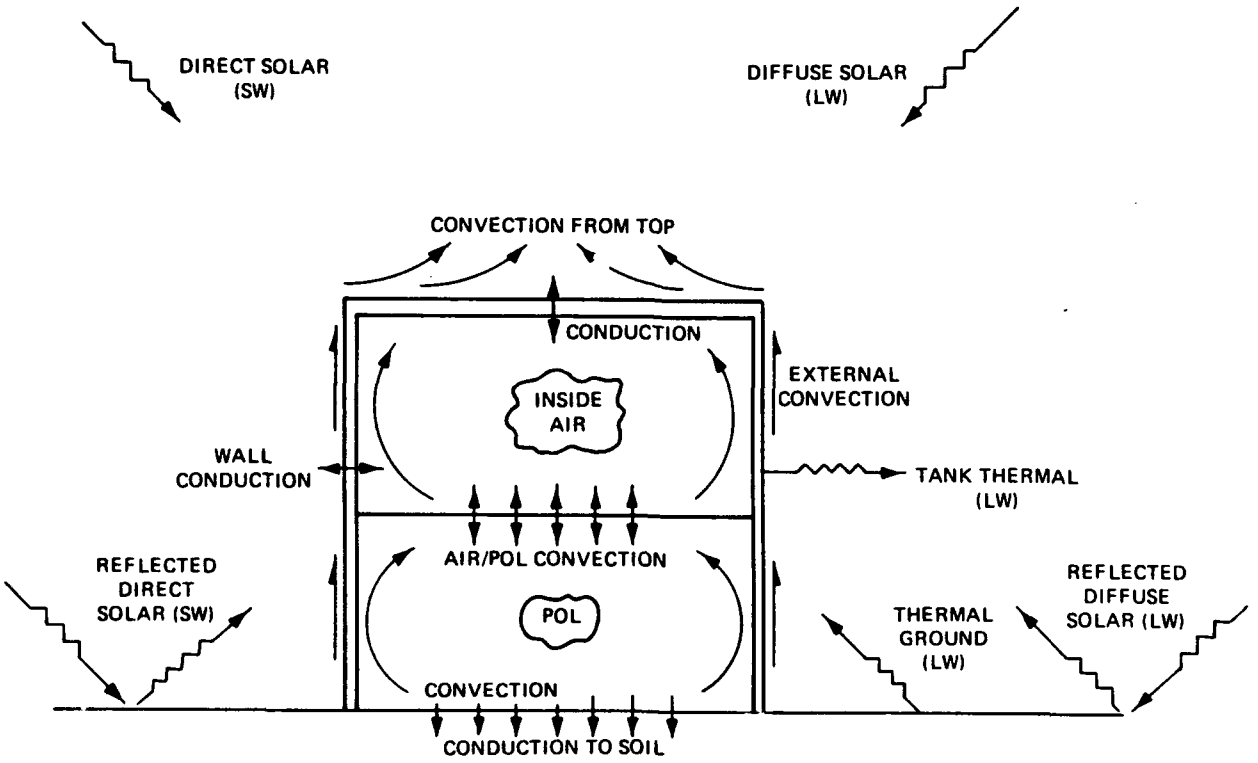

Figure 11. POL storage tank energy transfer mechanisms (SW = short-wave, LW = longwave)

from the masses. Energy transfer within the tank's metal structure is by conduction. Energy transfer to the tank's outside surfaces is by convection and radiation, and energy transfer to the air and liquid contained within the tank is by convection. Heat transfer to or from the soil is by conduction.

130. Models of varying sophistication can be developed to describe the time-dependence of the surface temperatures of the tank. Generally, the less sophisticated the model, the greater the empiricisms required and the more significant (and limiting) the assumptions involved. However, simple models that emulate the correct physics are capable of yielding quantitatively accurate results (Stoecker 1980). An examination of models of varying levels is provided below.

131. Perhaps the most sophisticated modeling approach for this problem would be to recognize its true 3-D, time-dependent nature and to model the conduction through the tank structure as well as the ground using a 3-D, time-dependent heat conduction computer code. In such an effort, the 3-D, time-dependent Navier-Stokes equations, with a turbulence model if needed, would be used to resolve the motion of the liquid and air (both internal and external) to define the convective heat transfer contributions to the tank structure and ground. The radiative heat transfer contributions would similarly be defined and resolved. Such an approach, which would require considerable computer resources, could be expected to model the process from a refined-as-possible theoretical basis, but the cost would be prohibitive for routine application. Such a model would not be easy to calibrate or to use since model output would be much more detailed (i.e., spatially and temporally) than any feasible set of experimental results. This approach is thus not tenable for target modeling requirements.

132. An alternative to the above approach is to make extensive use of lumped-parameter models based on salient physics. Following such an approach, four features must be modeled: (a) the air and liquid masses inside the tank, (b) the influence of the ground on the liquid mass, (c) the response of the tank structure, and (d) the convective and radiative heat transfer to the surfaces of the tank.

133. The air and liquid masses within the tank must be considered separately because of the great disparity in thermal capacity per unit volume (air is order of 10^3 J m^{-3} $°K^{-1}$ and oil is order of 10^6 J m^{-3} $°K^{-1}$). Thus, during the typical diurnal cycle, the liquid temperature would not vary more than a few degrees, while the inside air temperature would vary many degrees.

The net result is that the liquid tends to act as a constant temperature "sink" for the process while the inside air temperature follows (lags) the tank's surface temperatures. A reasonable modeling procedure is to treat the liquid and inside air as single masses, each with a single (average) temperature. The liquid and inside air temperatures would vary as prescribed by the thermal capacity and the net heat transfer to or from the individual masses. For these lumped-mass models, the convective heat transfer is based on a convective heat transfer coefficient with the driving potential being the difference between the lumped-mass temperature and the surface temperature. Existing or modified convective heat transfer correlations must be provided, as the lumped-mass approach does not define the heat transfer (as does the Navier-Stokes equations approach).

134. The ground provides additional mass that is available for energy interchange with the liquid (and outside air). Consistent with the lumped-mass assumption made for the air and liquid within the tank is the assumption that the energy transfer from the bottom of the tank to the soil is one-dimensional (i.e., constant across the bottom of the tank) and that the conduction within the soil is also one-dimensional. Effects of the soil heat conduction other than directly below the tank are ignored.

135. The major objective of this model is the prediction of the temperature on the surfaces of POL bulk storage tanks. Because of the high thermal conductivity (and consequently low thermal resistance), the tank walls can be treated in a lumped-mass fashion similar to that of the inside air and liquid. However, because of the low Biot number ($Bi < 0.02$) associated with the tank walls, this is a much better assumption for the walls than for the inside air and liquid (Kreith and Bohn 1986). Logic dictates that at least the tank top, tank bottom, and walls adjacent to the inside air and walls adjacent to the liquid be considered separately. Additionally, because of the diurnal motion of the sun, some distinction as to tank wall orientation must be made. The simplest viable division is to consider east, south, west, and north faces adjacent to the inside air and liquid; thus, eight wall portions and the tank top are considered. Each individual wall face is considered as isolated from the others so that no conductive path exists between tank wall faces.

136. The remaining feature to be considered involves the convective and radiative heat transfer to the outside surface of the tank (Incropera and de Witt 1981, Poulikakos 1985, Sparrow and Prata 1985, and Young and Ozel 1985). As with the inside air and liquid, the convective heat transfer can be

specified by existing heat transfer correlations, with the driving potentials being the differences between the outside ambient temperature and the surface temperatures. Because of the possibility of horizontal winds as well as vertical buoyancy forces, mixed free and forced convection effects must be accounted for on the exterior surfaces. For this problem, the dominant energy transfer mechanism is the solar-driven radiative heat transfer. Shortwave and longwave, direct and diffuse, contributions as well as thermal radiation from the ground and tank surfaces must be considered. Because of the sun path, various surfaces will be exposed to varying-intensity solar radiation as the day progresses (Weiss and Scoggins 1989).

137. Energy balances must be written for each of the 12 (tank top, tank bottom, eight wall segments, inside air, inside liquid) lumped-mass components introduced earlier. Each energy balance is based on conservation of energy as applied to a control volume; the general form is (Hodge 1989)

$$-\rho cVol \frac{dT}{dt} = \Sigma \dot{q} \tag{105}$$

where

$\rho cVol$ = thermal capacity of mass within control volume, W-sec

T = mass temperature, °C

t = time, sec

$\Sigma \dot{q}$ = summation of energy fluxes to and from control volume, W

The vertical wall target surface temperature model (Weiss and Scoggins 1989) was used to calculate the radiative flux on the fluid-filled target walls and to calculate the resulting physical temperature and radiance of the target surfaces. In this way, the radiance of POL tanks is predicted in terms of local weather conditions, terrain surface type, target surface emissivity and absorptivity, latitude, and time of day.

PART VI: RADAR SIGNATURES OF TERRAIN BACKGROUNDS

138. Knowledge of the interaction of electromagnetic waves with terrain features is important to discriminate targets from background features using active or passive radar sensors. An advantage of using millimeter or microwave radar systems as target locators is that they function reasonably well under adverse weather conditions such as cloud cover, mist, or fog where IR and visible light sensors lose their effectiveness. The main difficulty with using radar detectors is the discrimination of target signals from the background clutter; often the background clutter masks the target signal or causes false target alarms. Therefore, it is necessary to be able to predict the magnitude of the background clutter for various types of terrain textures such as soils, plowed fields, grass, forest canopies, and urban areas. The relative magnitude of a target signal and the background clutter depends on the operational characteristics of a radar transceiver system, such as the frequency and polarization of the transmitted and received waves, and on the depression angle of the transmitted waves.

139. The radar return signal from real terrain is generally due to the processes of reflection and scattering. Reflection is a surface effect while scattering occurs at rough surfaces or within the volume of the terrain texture material. The volume scattering is generally associated with the random variation of the structure of terrain materials about some average value. Both surface and volume scattering are important for natural terrain materials (Fung and Ulaby 1983) and can be described by differential scattering cross sections designated by σ_s and σ_v, respectively. The total differential scattering cross section is written as

$$\sigma = \sigma_s + \sigma_v \tag{106}$$

and the average power received by an antenna of an active radar sensor system is written as (Fung and Ulaby 1983)

$$P_r = \lambda^2/(4\pi)^3 \, P_t G_t G_r \int \sigma/R^4 \, dS \tag{107}$$

where

P_r = received power, W

λ = wavelength of electromagnetic radiation, m

P_t = transmitted power, W

G_t = gain of transmitting antenna

G_r = gain of receiving antenna

σ = differential cross section, $m^2\ m^{-2}$

R = distance between radar antenna and the scattering point on the terrain surface, m

S = area of radar footprint on terrain surface, m^2

140. From Equation 107 it is clear that the terrain characteristics enter the received power calculation through the values of the differential cross section. The differential cross section for the scattering of electromagnetic waves from terrain elements depends on a number of physical parameters:

a. Surface microroughness - small-scale terrain features.

b. Surface mesoroughness - medium-scale terrain features.

c. Wavelength of electromagnetic radiation.

d. Depression angles of receiver and transmitter.

e. Polarization of the transmitted and received signals--VV, VH, HV, HH.

f. Electrical properties of terrain elements--average values, standard deviations, and correlation lengths for the dielectric constant, magnetic permeability, and electrical conductivity.

The electrical properties of terrain elements are determined by soil and vegetation type, moisture content of soil and vegetation type, moisture content of soil and vegetation, wavelength of the electromagnetic waves, and soil and vegetation temperature.

141. Many models of varying complexity are available that can represent the differential scattering cross section of terrain textures in terms of the physical parameters listed in the above paragraph (Fung and Ulaby 1983). The model used in this report to create the Regional Radar Scattering Map is a random medium volume and rough surface radar wave scattering model for vegetation, soils, and snow cover (Zuniga, Habashy, and Kong 1979; Lee and Kong 1985a,b; Borgeaud, Shin, and Kong 1987).

142. A three-layer random medium model is developed to study the fully polarimetric scattering properties of earth terrain. The top layer is modeled

as an isotropic random medium, the middle layer as an anisotropic random medium, and the bottom layer as a homogeneous half-space. Volume scattering effects of both random media are characterized by correlation functions in which variances and correlation lengths describe strengths of permittivity fluctuations and physical sizes of embedded inhomogeneities, respectively. The anisotropic effect of the middle layer is attributed to specific structure and alignment of the scatterers. With the strong fluctuation theory, the mean fields in the random media are derived under the bilocal approximation with singularities of the dyadic Green's functions properly taken into consideration. With the discrete scatterer concept, effective permittivities of the random media are calculated by two-phase mixing formulas. Then, the distorted Born approximation is used to calculate the covariance matrix, which describes the fully polarimetric scattering properties of the terrain and is used in radar image simulation and earth terrain identification and classification (Lim et al. 1989, Kong et al. 1990).

143. A two-layer random medium model has been successfully applied to polarimetric remote sensing of earth terrain such as vegetation, meadow, and ice layer. The results obtained with the three-layer configuration have the capability of accounting for polarimetric scattering from earth terrain under the effects of weather, seasonal variation, and atmospheric conditions such as forest under mist, meadow under fog, and ice under snow. The effects on polarimetric wave scattering due to the top layer are identified by comparing the three-layer model results with those obtained from the two-layer model. The enhancement of the radar returns due to dry-snow cover on top of first-year sea ice observed in the experimental data can be explained using the three-layer random medium model. The theoretical results are illustrated by comparing the calculated covariance matrices with the polarimetric measurement data (Zuniga, Habashy, and Kong 1979).

144. The scattering of electromagnetic waves from a randomly perturbed periodic surface is formulated by the extended boundary condition (EBC) method and solved by the small perturbation method (SPM). The scattering from periodic surface is solved exactly, and this solution is applied in the SPM to solve for the surface currents and scattered fields up to the second order. The random perturbation is modeled as a Gaussian random process. The theoretical results are illustrated by calculating the bistatic and backscattering coefficients. It is shown that as the correlation length of the random roughness increases, the bistatic scattering pattern of the scattered fields shows

several beams associated with each Bragg diffraction direction of the periodic surface. When the correlation length becomes smaller, the shape of the beams becomes broader. The results obtained using the EBC/SPM method also compare with the results obtained from the Kirchhoff approximation. The Kirchhoff approximation results agree quite well with EBC/SPM method results for the HH and VV polarized backscattering coefficients for small angles of incidence. However, the Kirchhoff approximation does not give depolarized returns in the backscattering direction, whereas the results obtained using the EBC/SPM method give significant depolarized returns when the incident direction is not perpendicular to the row direction of the periodic surface (Yueh, Shin, and Kong 1988).

145. We have studied the Mueller matrix and polarization covariance matrix for polarimetric radar systems. The clutter is modeled by a layer of random permittivity, described by a 3-D correlation function, with variance, and horizontal and vertical correlation lengths. This model is applied, using the wave theory with Born approximations carried to the second order, to find the backscattering elements of the polarimetric matrices. It is found that 8 of 16 elements of the Mueller matrix are identically zero, corresponding to a covariance matrix with four zero elements. Theoretical predictions are matched with experimental data for vegetation fields (Borgeaud, Shin, and Kong 1987).

146. The vegetation canopy and snow-covered ice field have been studied with a three-layer model, an isotropic random medium layer overlying an anisotropic random medium. We have calculated the dyadic Green's functions of the three-layer medium and the scattered electromagnetic intensities with the Born approximation. The backscattering cross sections are evaluated for active microwave remote sensing. The theoretical approach can be extended to derive the bistatic scattering coefficients (Borgeaud, Shin, and Kong 1987).

PART VII: DEVELOPMENT OF LASER SCATTERING MODELS

Background

147. A parallel effort to develop laser scattering models to describe and predict the interaction of laser light with natural terrain backgrounds was initiated in January 1987. Development of a 1-D semi-empirical laser scattering model was initiated at WES by the members of the Background Signatures Team. A more comprehensive and ambitious theoretical model was contracted for development (Ishimaru 1978, Ma 1989).

Purpose and Scope

148. The objective of this research was to develop comprehensive and practical theoretical and semi-empirical models and computer codes for laser scene generation. Achieving this objective meant conducting extensive research in the following areas:

a. Development of a systematically comprehensive laser scattering model based on experience and research in the theories of wave scattering in random media. These scattering models are designed to predict the bidirectional reflectance for terrain textures such as soil, rocks, grass, trees, urban areas, agricultural areas, and other commonly occurring background types. These scattering models should also predict the bidirectional reflectance in terms of frequency, polarization, coherence, view angle, source angle, water content, weather, and season. These models are to be incorporated into a coarse-resolution regional map display and a fine-resolution laser scene display.

b. Development of a synthetic laser scene generation capability that will predict what a terrain background will look like to a laser scanner. This includes predictions of the correlation length and standard deviation of the spatial fluctuations of the scattered intensity for each type of terrain background texture.

c. Development of theoretical models to estimate the statistical variations, spatial correlations, and standard deviations of the scattered radiance from terrain in order to aid detection and identification of targets for the automatic target detection device under various weather conditions.

d. Incorporation of useful theoretical models to account for the atmospheric blurring effects due to dust, smoke, aerosols, clouds, and snow, including the modulation transfer function and the effects on spatial resolution and spatial frequencies.

e. Generation of useful and practical computer codes and graphics that can be used in the scene generation development program, data interpretations, and scene simulations, and regional map displays of characteristic laser scattering intensities as a function of terrain texture.

f. Development of data-calibrated, semi-empirical models to describe laser scattering from natural and man-made surfaces to meet near-term predictive requirements.

Semi-empirical Laser Scattering Model

149. The scattering properties of a rough terrain surface depend to a large degree on the following factors: laser altitude angle, sensor depression angle, average terrain roughness amplitude, and average terrain roughness wavelength (Bass and Fuks 1979, Mahrer 1982, Carroll 1982, and Weiss and Scoggins 1986). These factors will determine the fraction of the total terrain surface area that is illuminated, the fraction of the total terrain surface area that is viewed by the sensor, and the fraction of the viewed area that is illuminated or shaded. The fraction of the viewed area that is illuminated and shaded combined with the physical properties of the illuminated and shaded areas is used to calculate the scattering properties of rough terrain (Weiss and Scoggins 1986).

150. Initially, the terrain surface is assumed to have a sinusoidal variation of elevation. A first step toward calculating the scattering properties of rough terrain is to determine the fraction of a sinusoidal surface that is illuminated. Construction of a sensor view model required the development of two capabilities:

a. The prediction of the fraction of the rough terrain area that is viewed by a sensor for a specified depression angle (view altitude angle).

b. The prediction of the fraction of the viewed area that is illuminated.

The fraction of the viewed area that is lighted and shaded has the greatest influence in determining the laser scattering properties for rough terrain.

151. An analysis similar to one done to calculate the percentage of illuminated terrain area can be used to calculate the fraction of a rough terrain surface viewed by a sensor. The important physical quantity to calculate for evaluating sensor performance is the fraction of the viewed area that is illuminated. This fraction determines the effective scattering properties

of rough terrain that a sensor will detect in its field of view and the bi-directional reflectance for the case of a laser source and detector.

152. Rough terrain surfaces exhibit little specular reflection; therefore, a more realistic scattering formalism must be developed. The light-scattering model described in this paper can be applied to laser scattering from rough surfaces if the wavelength of the laser light is much smaller than the wavelength of the terrain elevation variation and also if the terrain roughness wavelength is less than the contact area of the laser beam with the terrain surface. In this case, the complex scattering process can be described by the bidirectional reflectance function. For a surface with no hidden areas, it is assumed that the scattering is purely Lambertian.

153. The rectilinear propagation model presented below describes, in general terms, the interaction of light with rough terrain surfaces (Weiss and Scoggins 1986; Meeker, Scoggins, and Weiss 1987; Meeker 1988). For laser scattering, this model predicts the effective scattering properties of rough terrain in terms of laser altitude angle, sensor depression angle, and the terrain roughness amplitude and wavelength.

154. Based on a 1 sinusoidally varying surface, the semi-empirical descriptive model calculates the fraction of the surface illuminated by the radiative source for a given incident angle. For a given view angle, the amount of illuminated area is determined, and the percentage of reflected radiation detected is calculated. The set parameters used to generate the descriptive curves can be broken down into three groups:

a. The amount of backward scattering is depicted through the use of the fraction illuminated calculation, and the forward scattering component is related by the fraction viewed calculation.

b. A term for diffuse reflection includes both the view angle and the incident angle, while the specular reflection term is dependent only on incident angle.

c. The backscatter and forward scatter segment of the model has a set of parameters to weight the scattering contributions appropriately, as determined by the experimental data for the particular class of material.

In addition, the three main groups all possess weighting coefficients of a similar nature which are related to each other in such a way that their sum is always equal to 1.

155. Critical inputs to the model include the wavelength of the incident radiation, the peak-to-peak amplitude of the sinusoid divided by its

wavelength, and the land use classification index number. These inputs combine to provide the model with flexibility in regard to surface roughness and spectral/reflectance characteristics for various types of soils, vegetation, and urban surfaces necessary for an accurate prediction of background signatures for the visible spectra.

Experimental Calibration of Laser Models

156. For an experiment in conjunction with the National Aeronautics and Space Administration's (NASA) Goddard Space Flight Center Code 623 and 300 laboratories, a goniometer was adapted to accommodate a HeNe laser, operating at 633 nm, and fiber-optic cable coupled to a silicon photodiode detector. A set of sample holders conforming to the National Bureau of Standards (NBS) specifications for bidirectional reflectance distribution function (BRDF) determination was constructed. The NBS employs powdered Halon pressed to a density of 1 g cm^{-3} as the reference for measuring BRDF; therefore, a powder press for Halon was constructed to NBS specifications. Actual data values were acquired through the use of a microcomputer set at a sample time of either 60 or 400 msec. All 400-msec data were acquired using a fiber-optic cable with lower transmission values than the cable used in the 60-msec measurements.

157. Data were acquired at 10-deg* intervals from -70 through 70 deg in the principal plane of incidence. In one set of samples, the angular increment was reduced to 2.5 deg, while some of the data runs made by NASA personnel were in 15-deg increments. Because of the configuration of the laser and the receiver, direct backscatter contributions could not be measured; therefore, measurements were made at 5 deg on either side of the incident angle.

158. The acquired data were then used to calibrate the WES laser scattering model. By setting constants in the model to control the relative contributions for various types of scattering as a function of the surface roughness parameters of amplitude and wavelength, the model output was adjusted to resemble the data curves. Thus, a semi-empirical method for the determination of the laser scattering characteristics function was constructed.

---

* To convert degrees (angle) to radians, multiply by 0.01745329.

PART VIII: BATTLEFIELD AIDS

159. A wide variety of electromagnetic sensors now exist for use in locating targets. These sensors operate by discriminating the target electromagnetic signatures from the terrain background electromagnetic signatures. Often the target is camouflaged so as to blend into the terrain background. The target and terrain electromagnetic signatures may be similar in a given waveband but different in other wavelengths of the electromagnetic spectrum. Very often, visual, infrared, and radar target locators will have different efficiencies for detecting targets that are hidden in complex terrain backgrounds. In addition, local weather conditions will severely affect the operational performance of some electromagnetic sensors. Therefore, it is important to have battlefield aids that will assist a commander in the selection of an appropriate electromagnetic sensor for specific targets, terrain backgrounds, and weather conditions.

160. The battlefield aids must be relatively simple so as to be mobile and operational under battlefield conditions. Therefore, the battlefield aids should be in the form of maps or images that can be displayed on a portable computer system; at the same time, they must be sufficiently sophisticated so as to utilize the characteristics of the target surface and the local terrain and weather conditions to make accurate multispectral predictions of the target/background signature contrast. The battlefield aids described in this report are based on the physical model that describes the interaction of electromagnetic waves with a target, terrain background, and sensor. These battlefield aids are presented in the form of color-coded maps, a synthetic scene generator, and a weather-dependent camouflage performance assessment algorithm. The battlefield aids considered in this report are as follows:

a. Regional elevation, slope, soil type, and land use map.

b. Regional thermal radiance map.

c. Regional radar cross section map.

d. Regional laser reflectance map.

e. Synthetic IR scene generator.

f. Camouflage Effectiveness Evaluation System.

These battlefield aids allow the user to estimate immediately the target location effectiveness of a specific sensor for a known type of target located in a specified terrain background.

Regional Signature Maps

161. WES has developed the capability to integrate thermal terrain signature models with terrain description data so that maps of signature values may be created for geographic regions of interest (Weiss and Scoggins 1989). Improvements have been made to the software to expand the accuracy of the thermal map by utilization of the WESTHERM combined surface model described earlier. Also, signature models for radar cross section and laser reflectance have been incorporated into map creation.

Background

162. Input databases. To produce a signature map of a specific geographic region, data describing the terrain surface shape and characteristics must be supplied. The terrain description data common to the signature maps are terrain elevation, land use, and soil types. Surface slope and azimuth (i.e., surface orientation relative to 0 deg north) are also necessary and can be supplied if available or calculated from the elevation data. Thus, five sets of regional description inputs are required. These data are in the form of digital maps that consist of 2-D arrays of numbers laid out on a regular grid. Each grid element is the value of the respective parameter at that geographical location. As an example, elevation could be specified on a 50-m grid, which means that the grid elements are the terrain elevation measured at regular points spaced 50 m apart horizontally and vertically. Whereas the elevation grid represents actual values in meters or feet, the land use and soil type grids will contain integer class numbers that are systematically assigned to specific feature types, such as land use class 4 for deciduous forest. Figure 12 contains example data for a site in Fort Hunter Liggett, California. Elevation, land use, and soil type for this site were digitized from maps; slope and azimuth were calculated from the elevation data.

163. In addition to the regional description database, another database of terrain physical properties must be available. This database is specific to the particular type of signature map desired. For thermal signature maps, soil thermal properties are one parameter that must be specified for each type of soil in the region. Alternatively, a laser reflectance map requires surface roughness for each land use in the land use data set. These data are cross-references to the class numbers in the land use and soil type data files so that, for any location in the region of interest, all parameters necessary to execute the specific signature model are known. Table 1 is a summary of

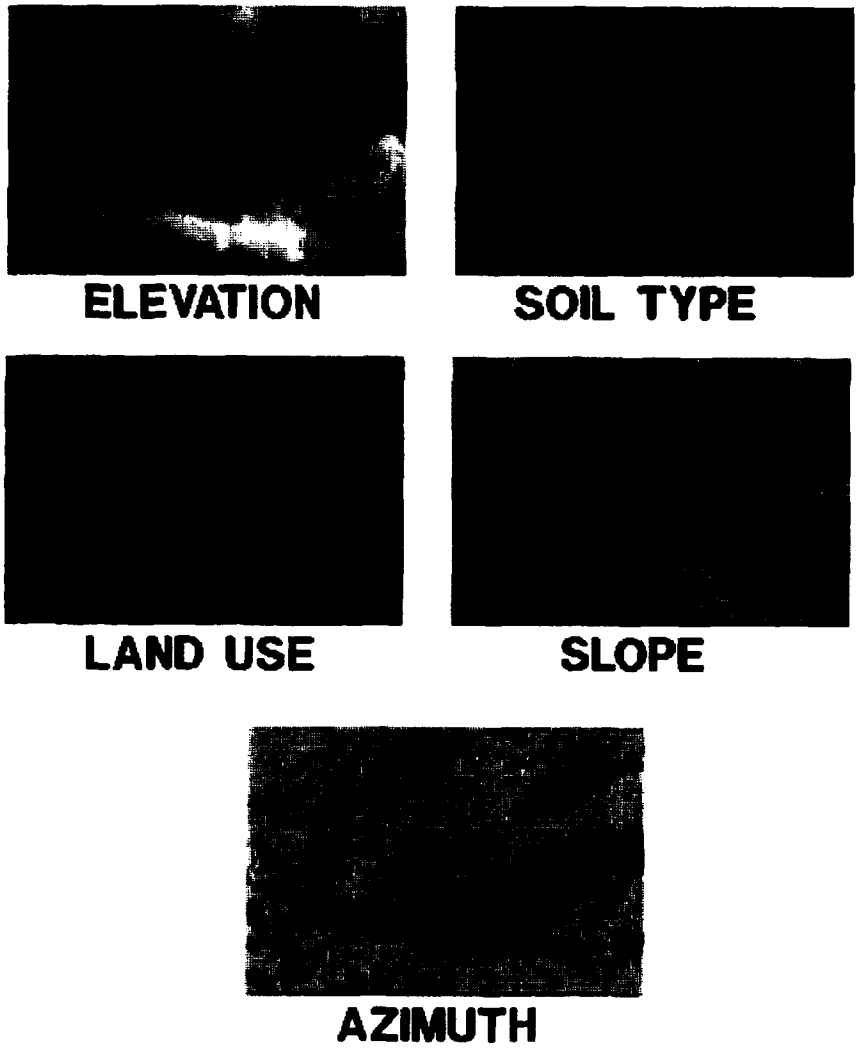

Figure 12. Geographic information system database

Table 1

Summary of Database Inputs for Signature Map Models

Thermal
Thermal conductivity
Thermal diffusivity
Surface/vegetation longwave emissivity
Surface/vegetation shortwave absorptivity
Surface moisture content
Vegetation cover factor
Vegetation height
Radar
Root-mean-squared surface slope
Complex dielectric constant
Layer thickness
Correlation length of dielectric constant
Laser
Characteristic surface roughness dimension
Surface roughness amplitude
Bidirectional reflection distribution function (optional)

the types of input required for the thermal, radar, and laser signature models.

164. One final type of input data is scenario-specific data entered by the user at the time of map generation. These data also depend on the particular type of map desired. A thermal map will require the user to enter the weather conditions near the time of interest. The radar and laser maps require sensor position, orientation, and operational wavelength.

165. Map generation. Given the presence of the databases described above, specific signature maps can be generated using software developed at WES (Weiss and Scoggins 1989). Improvements to WES software have been made to better account for surface slope and azimuth and to allow generation of radar cross-section and laser reflectance maps. The procedure by which the software produces the desired map is described below.

a. Scan terrain region description database to identify unique combinations of classes, called class vectors. This list is specific to the signature model and constitutes the number and type of model executions for the region. This is a one-time operation given that the region of interest does not change.

b. Repeatedly execute the desired signature model for the class vectors found in step a. These class vectors are cross-referenced to the parameter database to provide physical properties necessary for the model to generate a signature value. Create signature for each class vector.

c. Scan the elevation, land use, soil type, slope, and azimuth maps in parallel and produce a class vector for each grid element. Cross-reference the signature value to the element class vector. Create a new map by building a grid of signature values that are spatially registered with the terrain region description files.

Example maps

166. Figures 13-15 are examples of thermal, radar cross-section, and laser reflectance maps, respectively. These maps were produced for the Fort Hunter Liggett region represented by the terrain description maps shown in Figure 12. The thermal map represents the radiance from surfaces for a clear day in September at 1400 hr. Weather inputs used to produce Figure 13 are given in Table 2. The radar cross-section map (Figure 14) is for the same area for a system operating in the 35-GHz frequency band oriented at 45 deg relative to north and with an elevation of 15 deg from horizontal. Finally, the laser reflectance map (Figure 15) is for the Fort Hunter Liggett area illuminated by a laser operating at 1.06 μ with the same source orientation as with the radar. Unlike the radar, the laser map represents reflectance received by a sensor not at the source location. The sensor location for the laser map in Figure 15 is 335 deg relative to north and 15 deg relative to horizontal.

Thermal Infrared Computer Scene Generation

167. Surface temperature models allow simulation of temperatures for major terrain surface types. The models are implemented as subroutines to a driving program to facilitate temperature predictions of the surfaces on the terrain map. A specific terrain map is first scanned by a series of preprocessor programs, and a list of terrain types, azimuth angles, and slope angle classes is written to a file. Thus, when a scene is desired for specific weather conditions and time of day, this file is read by the model driver program for the necessary class combinations.

168. Based on the terrain type index (grass, trees, etc.), parameters needed by the appropriate model are extracted from a parameter database and passed to the correct model subprogram. The resulting temperatures are

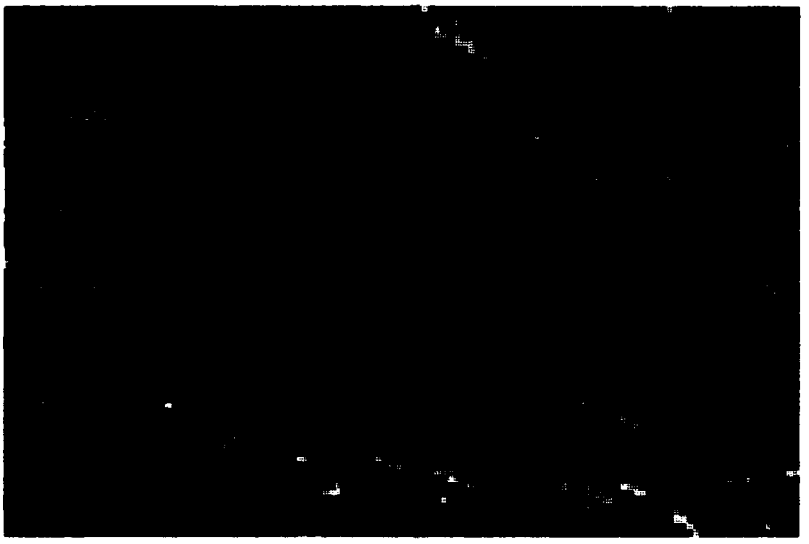

Figure 13. Regional thermal radiance map

Figure 14. Regional radar cross-section map

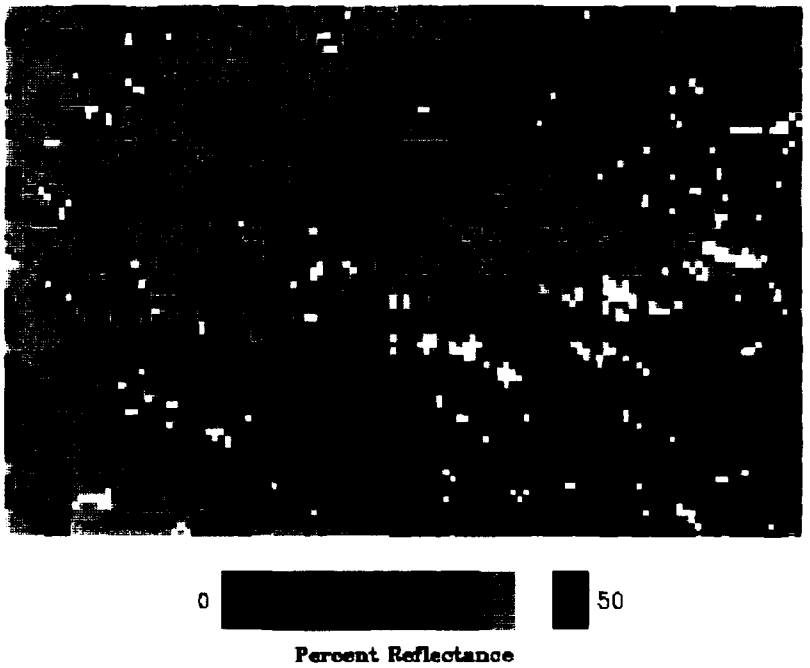

Figure 15. Regional laser reflectance map

Table 2

Weather Conditions Used for Regional Thermal Map Generation

Time hr	Air Temperature °C	Relative Humidity %	Cloud Cover %	Wind Speed m/sec
1	10.6	89	0	0.31
2	10.5	90	0	0.67
3	9.4	90	0	0.05
4	9.5	91	0	0.21
5	8.7	91	0	0.62
6	8.2	91	100	0.57
7	10.8	91	100	0.1
8	13.0	87	100	0.26
9	15.2	77	50	0.98
10	19.1	55	0	1.34
11	21.3	43	0	1.59
12	23.7	34	0	1.39
13	25.2	21	0	1.95
14	26.7	21	0	1.49
15	7.6	18	0	1.39
16	27.4	17	0	2.36
17	26.1	20	0	3.03
18	24.3	23	0	1.18
19	19.6	41	0	0.26
20	18.5	45	0	1.13
21	16.3	54	0	0.72
22	15.2	59	0	0.51
23	12.7	75	0	0.36
24	12.3	81	0	0.21

converted to blackbody radiances by an approximation equation (Weiss and Scoggins 1989). Values for the standard deviation and correlation length of radiance are selected from a list derived by analysis of actual thermal imagery of the particular texture type. Finally, the mean, standard deviation, and correlation length of the radiance for each surface type are written to an intermediate file for use by the scene generator software.

169. Such a scene generator is in use at WES for creation of simulated thermal IR scenes (Weiss and Scoggins 1989). Modules that degrade the "perfect" scene output by the scene generator software have been added to include the effects of the thermal sensor so that the final scene will more accurately reflect what would be displayed, such as on a monitor.

Scene Generator Program

Background

170. The structures of the objects and terrain backgrounds in the database which serve as input to the scene generator are approximated by triangular facets. The computer program reads the coordinates of all three vertices of the triangular facets from a file, along with the direction cosines of the normal of each facet. The direction cosines of the facets will be used by the program to determine which facets are seen from the sensor's point of view. Background surface-type information is derived from a digital terrain map. The terrain database is an encoding of information regarding the placement of background texture types. Finally, terrain surface boundary data, such as road edges, are inserted into the terrain map. These data are digitized from conventional maps and are merged in such a way that boundary coordinate data may be at a higher resolution than terrain facets. This final terrain map is the geometric model used by the scene generator for background scene production (Weiss and Scoggins 1989).

171. To construct a scene, the detector position, viewing direction, and orientation are specified in a data file. The angular field of view of the detector determines the footprint or scene size on the ground plane which is centered about the line of sight between the sensor and ground plane. The x, y, and z coordinates of the sensor relative to the origin of the terrain database must be entered into the scene generator program. In addition, the aspect angle, azimuth angle, and depression angle of the sensor must be specified. These parameters, along with sensor resolution and the size of the desired scene in number of pixels and rows, are entered into a file which is then read by the scene generator. This procedure defines one frame for the scene generator to create. The software is structured so that the parameter file is repeatedly read for additional frames for the scene generator to create until an end of file, at which point the program terminates.

172. The "brightness" of each scene pixel is related to the energy emitted, or radiance, from the terrain/object surfaces. Each facet is assigned a radiance value based on its texture type, which has been calculated by the surface temperature models, and standard deviations and correlation lengths that describe the variability of the texture type. In general, the intrinsic radiance of a surface depends on the orientation relative to the sun, the surface characteristics such as absorptivity and roughness, and the thermal inertia of the subsurface material.

Sensor model

173. The sensor model degrades the synthetic image created by the scene generator, accounting for the effects of sensor optics, detector response, and analog-to-digital conversion. The process consists of three main steps: transfer of the radiant energy flux through the sensor optics, conversion of the energy to voltage by the detector including scanning effects, and digitization of the voltage signal. Each of these steps removes detail from the perfect scene produced by the scene generator.

174. Modulation transfer function. The modulation transfer function accounts for the blurring effect of the sensor optics on the perfect image and calculates the irradiance incident on the detector element from each input pixel (Hudson 1969). Any optical system with a finite size aperture will blur a point source so that the image will be a spot rather than a point. Also, the irradiance, or energy incident on the detector, is a function of the sensor field of view as defined by the optics focal length. To account for this, a convolution or modulation of the input image with a 2-D Gaussian point-spread function is performed. The Gaussian function is defined by a mean related to the effective field of view and variances in the x and y dimensions that incorporate blurring effects. The calculation is given by

$$I_1(x,y) = \sum_{i=-m}^{+m} \sum_{j=-n}^{+n} I_0(x,y) \times G(x-i, y-j) \qquad (108)$$

where

I_1 = modified image

m,n = extent of convolution defined by variances

I_0 = original perfect image

G = zero mean Gaussian function

The mean variances, entered by the user, are related to specific characteristics of the optics such as the aperture, field stop, and lens diameter and are generally provided by the system manufacturer.

175. Detector voltage output. The next step in the sensor model is to calculate the voltage output from the sensor's detector element (Hudson 1969). This incorporates the responsivity of detector and scanning interlace in conversion of the irradiance to voltage. Responsivity is a wavelength-dependent constant for a detector material that relates the irradiance, in watts per square meter, to output voltage. Also, the noise imposed on the image by the detector can be calculated from responsivity and detector size.

176. Unlike a real image, which is a continuous brightness function, interlace effects occur when the scanning system does not exactly align the detector element on each pixel of the digital image produced by the scene generator. Also, the detector-optics combination may view an area greater than one scene pixel in size. To account for this properly, the initial scene must be generated at least twice the resolution of the final image, say at 200 by 200 pixels for a final image of 100 by 100 pixels. The higher resolution image is then resampled and averaged to a lower resolution to simulate this effect.

177. Digital-to-analog conversion. In most imaging sensor systems, the output voltage is converted to a number for display by computer on a monitor. An automatic gain control is normally used to adjust the dynamic range of the detector voltage to match the scale of the analog-to-digital conversion system, generally 0 to 255. This is done to optimize the contrast on the image finally displayed on the monitor. Such modeling simply amounts to scaling the values output by the detector-scanner simulation to the desired digital range.

Input specification and execution

178. To simulate a specific sensor system, details of the system must be entered into the sensor simulator. The system currently has data necessary to model the Inframetrics and AGA infrared scanners, with facilities for entering data to simulate other systems if such data are available. The scene generator itself is executed initially to produce the perfect image, requiring only the terrain and object geometry and view specifications (Weiss and Scoggins 1989). The sensor model utilizes the output of the scene generator to produce a degraded image that is a closer approximation to what would actually be seen on the monitor of scanning imager. Since the sensor model is a proto-processor, it is possible to use the software with other scene

generators, provided that the scene generator produces radiance values as output.

Camouflage Effectiveness Evaluation System (CEES)

Background

179. The CEES is a set of software that combines the thermal radiance prediction models for targets and terrain background with the Night Vision Laboratory Static Performance Model for Thermal Viewing Systems (Ratches et al. 1975) to obtain a model that predicts target detection probability at a specified range or target detection range for a 0.5 detection probability (Weiss and Scoggins 1989). The TSTM, VEGIE, and VCTM thermal models are used to predict terrain background radiance for use with IR sensors. CEES allows interactive specification of values for parameters such as emissivity, as well as other parameters that influence the surface temperature. The software is designed to allow for easy operation by the user and for output of the results in tabular as well as graphic form (Analytics, Inc. 1985). Primarily designed as a desktop tool for analysis of multispectral camouflage on fixed installations and other high-value targets, CEES has an input interface to aid the user in the evaluation and selection of model inputs. The following describes the incorporation of a passive millimeter wave (mmw) receiver model into CEES.

Technical approach

180. Surface signature models. CEES uses the WES thermal models to estimate background and target temperatures for analysis purposes. These models are executed as subroutines in the system and provide output for use by the sensor-specific portions of the systems. As described above, TSTM, VEGIE, and VCTM take as input meteorological data commonly collected by standard weather stations. These data are used to calculate a time-dependent surface boundary condition for use with a finite-difference formulation of the thermal conduction equation. Since the models predict physical temperatures, their output can be used by both the mmw and IR modules of the system performance calculations.

181. Passive millimeter wave model. The mmw model incorporated into the CEES program models a passive mmw receiver. A passive receiver detects the reflected and thermal radiation in the mmw spectral bank of bodies and materials that are at temperatures above absolute zero. The output of the mmw radiometer is proportional to the intensity of observed radiation within the

bandwidth of the receiver. The model determines effective temperatures for targets and backgrounds at various ranges based on (a) slant range to target, (b) target and background emissivities, (c) reflectance, and (d) atmospheric losses (clear, fog, rain).

182. The acquisition range is then calculated based on a minimum discernible temperature difference between the target and background. The mmw model was designed for an operating frequency of 36 GHz. However, it could easily be adopted to other frequencies if the emissivity and atmospherics tables for different materials at these frequencies were added.

183. The mmw model uses as inputs the physical temperatures for the target and background, calculated as described above with the WES thermal models. These are then attenuated through the atmosphere to obtain the effective temperatures at the sensor. The following equation is used to calculate effective temperatures while allowing for loss and self-emissions from the atmosphere.

$$T_{eff} = 10^{-\alpha \frac{R}{10}} \left(\epsilon T + (1 - \epsilon) T_s\right) + \left(1 - 10^{-\alpha \frac{R}{10}}\right) T_{amb} \qquad (109)$$

where

T_{eff} = effective temperature
R = slant range
ϵ = emissivity of target or background
T = physical temperature of target or background
T_s = sky temperature
α = atmospheric loss factor
T_{amb} = ambient temperature

The $10^{-\alpha(R/10)}$ term is the Beer's Law term to account for atmospheric effects in the millimeter wave spectral region (Poradish 1982).

184. The mmw model calculates acquisition ranges by initially setting the range to the sensor at 1 km and then increasing this distance in 5-km intervals until the target can no longer be acquired. Target acquisition is determined by comparing the difference between effective temperatures of the target and background at a given range with the minimum discernible ΔT value as input by the user. This value normally ranges from 0.1 to 10 °K. Once the

target acquisition range has been determined to within a 5-km interval, the interval size is reduced to 1 km, and the search continues until an acquisition range accurate to 1 km is determined.

PART IX: SUMMARY AND RECOMMENDATIONS

Summary

185. Several multispectral terrain background signature models have been described in this report. These models are based on physical principles and describe the interaction of electromagnetic waves with terrain backgrounds. The thermal models predict the physical temperature and the radiance of rough terrain backgrounds under ambient weather conditions for the relevant 3- to 5-μm and 8- to 14-μm wavebands. The radar scattering models calculate the differential scattering cross section of a rough terrain surface in terms of surface and volume scattering parameters, frequency, polarization (VV, VH, HV, or HH), and depression angles of the transmitter and receiver. In a similar manner, a laser scattering model is available that predicts bidirectional reflectance and surface depolarization for the scattering of laser light from rough terrain. These models have been incorporated into battlefield aids useful in assisting battlefield commanders to select the appropriate electromagnetic sensor system for given target, terrain, and weather conditions. The models that were developed are summarized below.

Thermal signature models

186. Terrain Surface Temperature Model (TSTM). This model predicts physical temperature and radiance of smooth nonvegetative surfaces in terms of time of day, ambient weather conditions, and radiative surface conditions such as emissivity and absorptivity, and in terms of heat conductivity and thermal diffusivity of the semi-infinite half-space used to represent the ground. An energy budget condition at the ground surface is used to determine the physical temperature at the ground surface, and a heat conduction equation is solved to obtain the subsurface temperatures. The basic physical processes of insolation, IR surface emission, absorption of IR radiation from the sky, heat conduction in the ground, convection heat loss to the atmosphere, and heat exchange due to evaporation and the formation of dew (phase changes) are considered in the surface energy budget condition.

187. Two-Dimensional Terrain Surface Temperature Model (2D-TSTM). This model is a 2-D version of the TSTM that predicts the physical temperature and radiance of smooth nonvegetative terrain surfaces but also allows for the possibility of lateral variation of the thermal properties of the ground. The physical principles for this model are essentially the same as for the TSTM.

188. Vegetative Surface Temperature Model (VEGIE). This model predicts the physical temperature and radiance of grass. It is a subprogram of the TSTM and extends this model by adding a thin layer of vegetation over the ground surface. Thermal IR energy is reflected back and forth between the two surfaces of this layer, and energy budget conditions are imposed simultaneously at the top and bottom surfaces of the layer. In this way, the physical temperature and radiance at the top surface can be determined using the basic principles of the TSTM.

189. Vegetation Canopy Temperature Model (VCTM). This model predicts the physical temperature and radiance of tree canopies. The model is a plane-parallel abstraction of a vegetation canopy that is divided into three horizontal layers. The radiation transfer equation is solved for this system subject to energy budget conditions at each of the boundaries. No heat storage is allowed within the canopy. Detailed canopy geometry information is required for each layer, including leaf area index and leaf slope distribution. In addition, the emission and absorption characteristics of the ground and canopy vegetation and the canopy stomatal resistance to water vapor diffusion are required to be known parameters.

190. Rough Terrain Surface Temperature Model (RTSTM). This model is an extension of the basic TSTM/VEGIE model to the case of a rough surface described by an average amplitude and a correlation length. The thermal radiance is calculated by evaluating the fraction of the area viewed by an IR sensor that is sunlit. Because this fraction depends on both the depression angle of the sensor and the altitude angle of the sun, it follows that the predicted radiance values also depend on these two angles. The standard input parameters for the TSTM/VEGIE model are also required to run the RTSTM.

191. Vertical Wall Target Surface Temperature Model (VWTSTM). This model is an extension of the TSTM to the case of a vertical wall of a solid body. For the case of a vertical wall, additional radiative fluxes arise due to reflected visible and IR radiation from the ground to the wall. In addition, there is the IR ground emission term that impinges on the wall. The model determines the physical temperature and radiance of the vertical walls of solid body targets.

192. Fluid-Filled Target Surface Temperature Model (FFTSTM). This model predicts the physical temperature and radiance of the vertical wall of a fluid-filled target such as a POL tank. The FFTSTM is essentially the VWTSTM with a convective heat transfer process replacing the heat conduction

mechanism. The FFTSTM can be used to evaluate camouflage applied to buildings such as aircraft shelters.

Radar model

193. The model predicts the differential scattering cross section of vegetative and nonvegetative surfaces in terms of surface roughness parameters and in terms of the physical structure of the terrain elements. This model is a full wave solution of Maxwell's equations for electromagnetic waves scattering in random media such as soils and vegetation. The electromagnetic structure of terrain materials is represented by mean values of the dielectric constant and the magnetic permeability and by the standard deviations and correlation lengths for these quantities. The differential scattering cross section is predicted for a frequency range of 0 → 100 GHz for any value of the depression angles of the receiver and transmitter and for the four possible transmitter and receiver polarization modes--HH, HV, VH, and VV.

Laser models

194. The development of models that describe the scattering of laser light from real terrain features such as soils, grass, leaves, bushes, and trees has proceeded in two directions: (a) an in-house research program to develop a semi-empirical laser scattering model and (b) a contracted research program to develop a rigorous, physically based laser scattering model. The semi-empirical model is based on the amount of scattering area available in the field of view of a laser sensor. This is calculated using a sinusoidal representation of the rough terrain surface and calculating the fraction of the viewed area illuminated by the laser. In this way, the bidirectional reflectance is predicted in terms of the depression angles of the laser and the detector. The more fundamental laser scattering model considers both volume and surface scattering and assumes the soil and vegetation to be random media. A radiative transfer assumption approximates the solution of Maxwell's equations for the scattering of light in the media.

Battlefield aids

195. The models described earlier in this report have been incorporated into various visual displays that can be used as battlefield aids to field commanders who must select the most appropriate weapon sensor system for known target, background, and weather conditions. The battlefield aids are developed to operate on PC-type computers in order to have the mobility that field units require.

196. The battlefield aids developed at WES include:

a. Regional elevation, slope, and land use maps. These maps display the elevation, slope and type of terrain for each region within the boundaries of the maps by using a color-coded scheme to indicate elevation, slope, and land use. Generally, a 100-m grid system is used, but for some areas data are available on a 20-m grid.

b. Regional thermal radiance map. The terrain temperature and radiance prediction models TSTM, VEGIE, and VCTM are applied to each area of known elevation, slope, and land use type, and the radiance and physical temperature are calculated. A color code displays the thermal properties of each area within the map. These maps can be generated for any time of day and night and for the weather conditions expected during the time of engagement with a target. This battlefield aid can select the proper thermal camouflage for military equipment and structures. It can also estimate the expected thermal contrast an enemy target will have at the time of engagement.

c. Regional radar cross-section map. The empirical terrain radar cross-section prediction model developed at WES has been combined with the terrain land use map to create a color-coded radar cross-section map that displays the magnitude of the differential scattering cross section of the various terrain elements of the background of a target. In this way the expected conspicuity of an enemy target can be estimated for a given radar system. On the other hand, the radar cross-section color map can be used to select proper camouflage against aircraft radars.

d. Regional laser reflectance map. The WES semi-empirical laser reflectance prediction model was joined to the terrain land use map in order to produce a laser reflectance map that uses a color-coded scheme to represent the magnitude of the reflectance for each terrain type in the area of interest.

e. Synthetic IR scene generation. The terrain elevation, slope, and land use database, together with the physically based terrain surface temperature prediction models, have been combined with a scene generation computer program to produce a synthetic IR target in background scene generation capability. The scene generation program consists of a target geometry model and a background geometry model that construct the target and background in terms of planar triangular facets. The angular field of view of the IR detector determines a footprint on the ground plane characterized by the triangular facets. Each triangular terrain facet is associated with a terrain texture type and slope, and the TSTM, VEGIE, and VCTM models are invoked to calculate the radiance of each facet. The TSTM is used to calculate the radiance of the target facets. The radiance of each facet depends on its orientation to the sun, consequently introducing a time dependence to the radiance of the facets as the sun moves across the sky. Additional time dependence is introduced by a varying air temperature. The effects of weather are introduced through the basic

TSTM program, which includes effects of cloud cover and cloud type. An EOSAEL subprogram accounts for the attenuation of the IR image as it is projected through the atmosphere. In this way, a time-dependent and weather-dependent synthetic IR image of a target in a realistic background can be created.

f. Camouflage Effectiveness Evaluation System. The CEES is a set of software that combines the thermal radiance prediction models for targets and terrain backgrounds with the Night Vision Laboratory Static Performance Model for Thermal Viewing Systems to obtain a model that predicts target detection probability at a specified range or target detection range for a 0.5 target detection probability. The TSTM calculates the target radiance, while the TSTM, VEGIE, and VCTM predict terrain background radiance. The target and background radiance contrast depends on the relative values of the corresponding surface emissivities, as well as the surface temperature values. Therefore, the CEES allows the user to select the value of the target surface emissivity that minimizes the target-background thermal contrast and hence minimizes the target detection probability for any time of day and ambient weather conditions.

Recommendations

197. This study of IR, radar, and laser target detection models and the associated battlefield aids has produced the following recommendations:

a. An experimental study should be undertaken to evaluate the terrain signature models and battlefield aids described in this report.

b. Signature models for high-value targets should be improved and embellished.

c. Methods of improving target detection under severe weather conditions should be studied.

REFERENCES

Analytics, Inc. 1985. "Camouflage Effectiveness Evaluation System," Technical Memorandum 1900-03, prepared for the US Army Engineer Waterways Experiment Station, Vicksburg, MS.

Baird, A. M., D'Argenio, C. S., Greenwood, F. C., and Bloomer, R. 1982. "Computer Generation of Realistic Infrared Scenes of Ground Targets in Environmental Backgrounds," Analytics Corporation, Willow Grove, PA.

Balick, L. K., Link, L. E., Scoggins, R. K., and Solomon, J. L. 1981. "Thermal Modeling of Terrain Surface Elements," Technical Report EL-81-2, US Army Engineer Waterways Experiment Station, Vicksburg, MS.

Balick, L. K., Scoggins, L. E., and Link, L. E. 1981. "Inclusion of a Simple Vegetation Layer in Terrain Temperature Models for Thermal Infrared (IR) Signature Prediction," Miscellaneous Paper EL-81-4, US Army Engineer Waterways Experiment Station, Vicksburg, MS.

Bass, F. G., and Fuks, I. M. 1979. Wave Scattering from Statistically Rough Surfaces, Pergamon Press, New York.

Borgeaud, M., Shin, R. T., and Kong, J. A. 1987. "Theoretical Models for Polarimetric Radar Clutter," Journal of Electromagnetic Waves and Applications, Vol 1, pp 61-77.

Bornemeier, D., Bennett, R., and Horvath, R. 1969. "Target Temperature Modeling," prepared by the Infrared and Optics Laboratory of Willow Run Laboratories, University of Michigan, for Rome Air Development Center, Griffiss Air Force Base, New York.

Botkin, E., Kelley, G., Gawronski, G., Krassner, J., Klop, M., Golman, R., Baird, A., and D'Argenio, C. 1981. "Infrared Modeling and Analysis (IRMA) Technical Report; Vol I: Scene Generation and Sensor/Seeker Interface," Report AFATL-TR-81, Air Force Armament Laboratory, Eglin Air Force Base, Florida.

Budyko, M. I. 1974. Climate and Life, Academic Press, New York.

Carroll, I. 1982. The Effect of Surface Striations on the Absorption of Shortwave Radiation, Journal of Geophysical Research, Vol 87, No. C12, pp 9647-9652.

Deardorff, J. W. 1978. "Efficient Prediction of Ground Surface Temperature and Moisture, with Inclusion of a Layer of Vegetation," Journal of Geophysical Research, Vol 83, pp 1889-1904.

Fung, A. K., and Ulaby, F. T. 1983. "Matter-Energy Interaction in the Microwave Region," Manual of Remote Sensing, Vol 1, American Society of Remote Sensing, New York, NY.

General Electric Company. 1975. Heat Transfer and Fluid Flow Data Books, Schenectady, NY.

Gillespie, A. R., and Kahle, A. B. 1977. "Construction and Interpretation of a Digital Thermal Inertia Image," Photogrammetric Engineering and Remote Sensing, Vol 43, No. 8, pp 983-1000.

Hechinger, E., Raffy, M., and Becker, F. 1982. "Comparison Between the Accuracies of a New Discretization Method and an Improved Fourier Method to Evaluate Heat Transfers Between Soil and Atmosphere," Journal of Geophysical Research, Vol 87, No. C9, pp 7325-7339.

Hodge, B. K. 1989. "Thermal Modeling of Petroleum, Oil, and Lubricants (POL) Bulk Storage Tanks," Technical Report EL-89-4, US Army Engineer Waterways Experiment Station, Vicksburg, MS.

Holter, M. R., Nudelman, S., Suits, G. H., Wolfe, W. L., and Zissis, G. J. 1962. Fundamentals of Infrared Technology, Macmillan, New York.

Hudson, R. D. 1969. Infrared Systems Engineering, John Wiley and Sons, New York.

Incropera, F. P., and de Witt, D. P. 1981. Fundamentals of Heat Transfer, John Wiley and Sons, New York.

Ishimaru, A. 1978. Wave Propagation and Scattering in Random Media, Vols 1 and 2, Academic Press, New York.

Jacobs, P. A. M. 1980. "Simulation of the Thermal Behavior of an Object and Its Nearby Surroundings," Report PHL 1980-08, Physics Laboratory of the National Defense Research Organization, TNO, The Hague, Netherlands.

Jamieson, J. A., McFee, R. H., Plass, G. N., Grube, R. H., and Richards, R. G. 1963. Infrared Physics and Engineering, McGraw-Hill, New York.

Kahle, A. B. 1977. "A Simple Thermal Model of the Earth's Surface for Geologic Mapping by Remote Sensing," Journal of Geophysical Research, Vol 82, No. 11, pp 1673-1680.

Kays, M. D., Seagraves, M. A., Monahan, H. H., and Sutherland, R. A. 1980. "Qualitative Descriptions of Obscuration Factors in Central Europe," ASL Monograph No. 4, US Army Atmospheric Sciences Laboratory, White Sands Missile Range, NM.

Kong, J. A., Yueh, S. H., Lim, H. H., Shin, R. T., and Zyl, J. J. 1990. "Classification and Maximum Contrast of Earth Terrain Using Polarimetric Synthetic Aperture Radar Images," Progress in Electromagnetic Research, Vol 3, Chap 6, Elsevier, New York.

Kreith, F., and Bohn, M. S. 1986. Principles of Heat Transfer, 4th ed., Harper and Row, New York.

Kruse, P. W., McGlaughlin, L. D., and McQuistan, R. B. 1962. Elements of Infrared Technology, John Wiley, New York.

Lee, J. K., and Kong, J. A. 1985a. "Active Microwave Remote Sensing of an Anisotropic Random-Medium Layer," IEEE Transactions on Geoscience and Remote Sensing, Vol GE-23, No. 6, pp 910-923.

_____. 1985b. "Passive Microwave Remote Sensing of an Anisotropic Random-Medium Layer," IEEE Transactions on Geoscience and Remote Sensing, Vol GE-23, No. 6, pp 924-932.

Lim, H., Swartz, A. A., Yueh, H. A., Kong, J. A., Shin, R. T., and Zyl, J. J. 1989. "Classification of Earth Terrain Using Synthetic Aperature Radar Images," Journal of Geophysical Research, Vol 94, No. B6, pp 7049-7057.

Link, L. E. 1979. "Thermal Modeling of Battlefield Scene Components," Miscellaneous Paper EL-79-5, US Army Engineer Waterways Experiment Station, Vicksburg, MS.

Ma, Q. 1989. "Study of Scattering and Depolarization of an Electromagnetic Wave Incident Upon a Slab of Random Medium Using Radiative Transfer Theory," Ph.D. dissertation, University of Washington, Seattle.

Mahrer, Y. 1982. "A Theoretical Study of the Effect of Soil Surface Shape Upon the Soil Temperature Profile," Soil Science, Vol 134, No. 6.

Meeker, D. L. 1988. "Laser Scattering from Rough Surfaces--Characterization and Prediction," 57th Military Operations Research Society Symposium Proceedings, MORS, Washington, DC.

Meeker, D. L., Scoggins, R. K., and Weiss, R. A. 1987. "Regional Electromagnetic Maps for Remote Sensing," Eighth Annual EOSAEL/TWI Conference, US Army Atmospheric Sciences Laboratory, Las Cruces, NM.

Poradish, F. J. 1982. Ka-Bank Passive/Active Airborne Radar, NAECON Record, US Army Engineering Topographic Laboratory, Fort Belvoir, VA, pp 1262-1269.

Poulikakos, D. 1985. "Natural Convection in a Confined Fluid-Filled Space Driven by a Single Vertical Wall with Warm and Cold Regions," Transactions, American Society of Mechanical Engineers, Journal of Heat Transfer, Vol 107, pp 867-876.

Ratches, J. A., et al. 1975. "Night Vision Laboratory Static Performance Model for Thermal Viewing Systems," Report ECOM-7043, US Army Night Vision and Electro-Optics Laboratory, Fort Belvoir, VA.

Rounds, E. M., Zavodny, A. T., and Mazzer, M. A. 1980. "Sensor Simulation of Natural Scenes," Fourth International Computer Software and Applications Conference, US Army Night Vision and Electro-Optics Laboratory, Fort Belvoir, VA.

Smith, J. A., Ranson, K. J., Nguyen, D., and Link, L. E. 1980. "Thermal Vegetation Canopy Model Studies," Colorado State University, Fort Collins, CO.

Solomon, J. L. 1982. "A Two-Dimensional Model to Describe Heat Flow in Terrain Materials," prepared by Mississippi State University for US Army Engineer Waterways Experiment Station, Vicksburg, MS.

Sparrow, E. M., and Prata, A. T. 1985. "Effects of Circumferential Conduction on the Critical Radius of Insulation for Forced Convection Crossflow," Transactions, American Society of Mechanical Engineers, Journal of Heat Transfer, Vol 107, pp 960-963.

Stoecker, W. F. 1980. Design of Thermal Systems, 2d ed., McGraw-Hill, New York.

Weiss, R. A. 1981. "Terrain Microroughness and the Dynamic Response of Vehicles," Transactions, 27th Conference of Army Mathematicians, ARO Report 82-1, US Army Research Office, Research Triangle Park, NC.

_____. 1982. Terrain Mesoroughness and Its Application to Mobility and Cover, Transactions, 28th Conference of Army Mathematicians, ARO Report 83-1, US Army Research Office, Research Triangle Park, NC.

Weiss, R. A., and Scoggins, R. K. 1986. "Light and Shadow Effects in Rough Terrain," 7th EOSAEL/TWI Conference, US Army Atmospheric Sciences Laboratory, Las Cruces, NM.

_____. 1989. "Infrared Target Background Analytical Models," Technical Report EL-89-11, US Army Engineer Waterways Experiment Station, Vicksburg, MS.

Young, M. F., and Ozel, T. 1985. "Mixed Free and Forced Convections from a Short Vertical Cylinder Placed in a Laminar Horizontal Flow," Transactions, American Society of Mechanical Engineers, Journal of Heat Transfer, Vol 107, pp 250-254.

Yueh, H. A., Shin, R. T., and Kong, J. A. 1988. "Scattering of Electromagnetic Waves from a Periodic Surface with Random Roughness," Journal of Applied Physics, Vol 64, No. 4, pp 1657-1670.

Zavodny, A. T., and Mazzer, M. A. 1980. "Simulation of Cultural Scenes for Passive Infrared Sensors," Fourth International Computer Software and Applications Conference, US Army Night Vision and Electro-Optics Laboratory, Fort Belvoir, VA.

Zuniga, M. A., Habashy, T. M., and Kong, J. A. 1979. "Active Remote Sensing of Layered Random Media," IEEE Transactions on Geoscience Electronics, Vol GE-17, No. 4, pp 296-302.

Waterways Experiment Station Cataloging-in-Publication Data

Weiss, Richard A.
Terrain background signature research / by Richard A. Weiss, Randy K. Scoggins, David L. Meeker ; prepared for Department of the Army, US Army Corps of Engineers.
95 p. : ill. ; 28 cm. — (Technical report ; EL-92-32)
Includes bibliographical references.
1. Infrared detectors — Military aspects. 2. Target acquisition. 3. Military geography — Remote sensing. 4. Infrared imaging — Military aspects. I. Scoggins, Randy K. II. Meeker, David L. III. United States. Army. Corps of Engineers. IV. US Army Engineer Waterways Experiment Station. V. Title. VI. Series: Technical report (US Army Engineer Waterways Experiment Station) ; EL-92-32.
TA7 W34 no.EL-92-32